Batteries & Supercaps

Review
doi.org/10.1002/batt.202400539

Chemistry Europe
European Chemical Societies Publishing

www.batteries-supercaps.org

Model-Driven Manufacturing of High-Energy-Density Batteries: A Review

Daria Maksimovna Vakhrusheva[a, b] and Jun Xu*[a, b]

The rapid advancement in energy storage technologies, particularly high-energy density batteries, is pivotal for diverse applications ranging from portable electronics to electric vehicles and grid storage. This review paper provides a comprehensive analysis of the recent progress in model-driven manufacturing approaches for high-energy-density batteries, highlighting the integration of computational models and simulations with experimental manufacturing processes to optimize performance, reliability, safety, and cost-effectiveness. We systematically examine various modeling techniques, including electrochemical, thermal, and mechanical models, and their roles in elucidating the complex interplay of materials, design, and manufacturing parameters. The review also discusses the challenges and opportunities in scaling up these model-driven approaches, addressing key issues such as model validation, parameter sensitivity, and the integration of machine learning and artificial intelligence for predictive modeling, process optimization, and quality assurance. By synthesizing current research findings and industry practices, this paper aims to outline a roadmap for future developments in model-driven manufacturing of high-energy density batteries, emphasizing the need for interdisciplinary collaboration and innovation to meet the increasing demands for energy storage solutions.

1. Introduction

Lithium-ion batteries (LIBs), known for their high energy density, longevity, and lightweight, have become a critical element in the modern battery industry (Figure 1). The journey began 30 years ago with Sony commercializing the world's first rechargeable LIB, inspired by the groundbreaking work of Yoshino.[1] The profound impact of this innovation was celebrated in 2019 when John B. Goodenough, M. Stanley Whittingham, and Akira Yoshino were honored with the Nobel Prize in Chemistry for their contributions to the development of lithium-ion batteries.

The surge in e-mobility (Figure 2) has catalyzed advancements in portable electronics, electric vehicles, and grid-scale energy storage systems. As a sustainable and wireless energy source, LIBs hold promise for mitigating global warming, evidenced by electric vehicles' lower greenhouse gas emissions compared to their petrol and diesel counterparts. Despite their eco-friendly allure, the manufacturing processes of LIBs are energy-intensive and contribute to greenhouse gas emissions, necessitating a critical reassessment and optimization to align with global environmental goals, *e.g.*, European Commission's 2035 goal for zero emissions from new vehicles.[2] Traditional manufacturing of LIBs includes steps of electrode preparation, cell assembly, and battery electrochemistry activation, requiring 20.3–37.5 kWh_{prod} amount of available energy, and produces 1 kWh_{cell} of cell energy.[3]

In the quest to address these challenges, model-driven manufacturing emerges as a groundbreaking paradigm, poised to redefine the landscape of high-energy density battery production. This innovative approach harnesses the power of sophisticated computational models and simulations to enhance every aspect of the manufacturing process, from the meticulous selection of materials and the intricate design of battery cells to the streamlined assembly processes and stringent quality assurance protocols. The integration of cutting-edge technologies such as artificial intelligence (AI), machine learning (ML), and comprehensive physics-based modeling not only facilitates a profound understanding of the complex interactions among various manufacturing parameters but also unveils opportunities for optimizing battery performance, reliability, and cost-efficiency.

This review paper endeavors to present an exhaustive examination of the latest advancements and methodologies in model-driven manufacturing for high-energy density batteries. It will meticulously explore the diverse array of modeling techniques currently employed within the industry, encompassing electrochemical, thermal, and mechanical models, as well as AI and ML-driven simulations. The paper will critically assess the efficacy and limitations of these models, illuminating their pivotal role in refining battery design, augmenting production efficiency, minimizing both costs and environmental impacts, and improving quality assurance. Additionally, the review will delve into the prospective future directions of model-driven manufacturing, discussing emergent trends, potential innovations, and the indispensable role of cross-disciplinary collaboration in propelling the field forward. By aggregating and analyzing the extensive body of knowledge and research findings within this domain, the paper aspires to provide

[a] D. Maksimovna Vakhrusheva, J. Xu
Department of Mechanical Engineering, University of Delaware, Newark, DE 19716 USA
E-mail: junxu@udel.edu

[b] D. Maksimovna Vakhrusheva, J. Xu
Energy Mechanics and Sustainability Laboratory (EMSLab), University of Delaware, Newark, DE 19716 USA

Review
doi.org/10.1002/batt.202400539
Chemistry Europe
European Chemical Societies Publishing

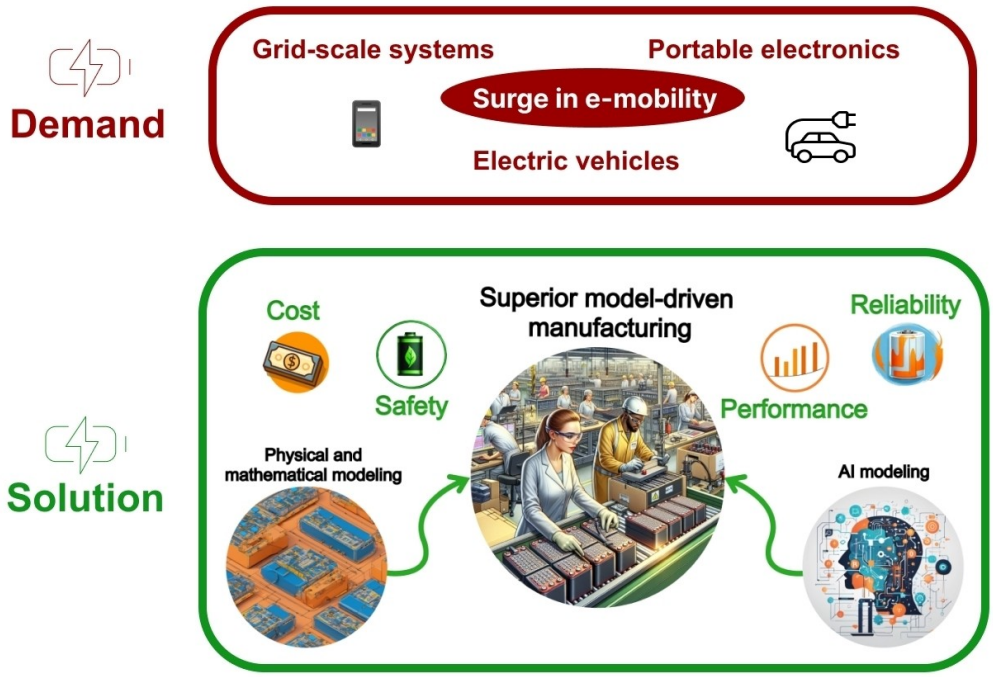

Figure 1. Demand for high-energy density batteries and the solution to provide commercial solutions by considering of performance, safety, durability and cost.

invaluable insights and guidance to a diverse audience, including researchers, engineers, industry practitioners, and policymakers engaged in the development and manufacturing of high-energy density batteries. It aims not only to elucidate the current state of the art but also to inspire and galvanize future research and development endeavors, with the ultimate goal of fostering more sustainable, efficient, and economically viable battery manufacturing solutions.

2. Understanding Battery Types and Their Composition

2.1. Anode

A typical battery structure contains cathode, anode and separator (Figure 3(a)). The anode is typically made of graphite, while there is ongoing research to develop alternative materials that could enhance battery performance, energy density, and cycle life. Some of the potential materials for anodes include metal lithium, elements of the 14th group, and lithium titanate.

Graphite anodes are widely used due to their stability, low cost, and relatively high energy density.[4,5] These electrodes

Daria is a PhD student at the Department of Mechanical Engineering, University of Delaware. She obtained her B.S.-M.S. degree at D. Mendeleev University of Chemical Technology of Russia (major in Fundamental and Applied Chemistry, working at N.D. Zelinsky Institute of Organic Chemistry, Russian Academy of Sciences). Her research interest is in a broad area of anode materials, with a focus on silicon ones for lithium-ion batteries and safe electrolytes for sodium-ion batteries.

Dr. Jun Xu currently is an Associate Professor (tenured) in the Department of Mechanical Engineering at the University of Delaware (UD), and Director of Energy Mechanics and Sustainability Laboratory (EMSLab). Dr. Xu is a Member at ASME, Senior Member at IEEE, and Member at SAE.
Dr. Xu obtained his Ph.D. from the Department of Earth and Environmental Engineering at Columbia University in 2014 (major in Environmental Engineering and Engineering mechanics).
His research expertise sits in the physics-based and data-driven modeling and characterization of battery safety, durability, design and manufacturing. Dr. Xu also has expertise in advanced design and understanding of materials and structures upon dynamic loading.

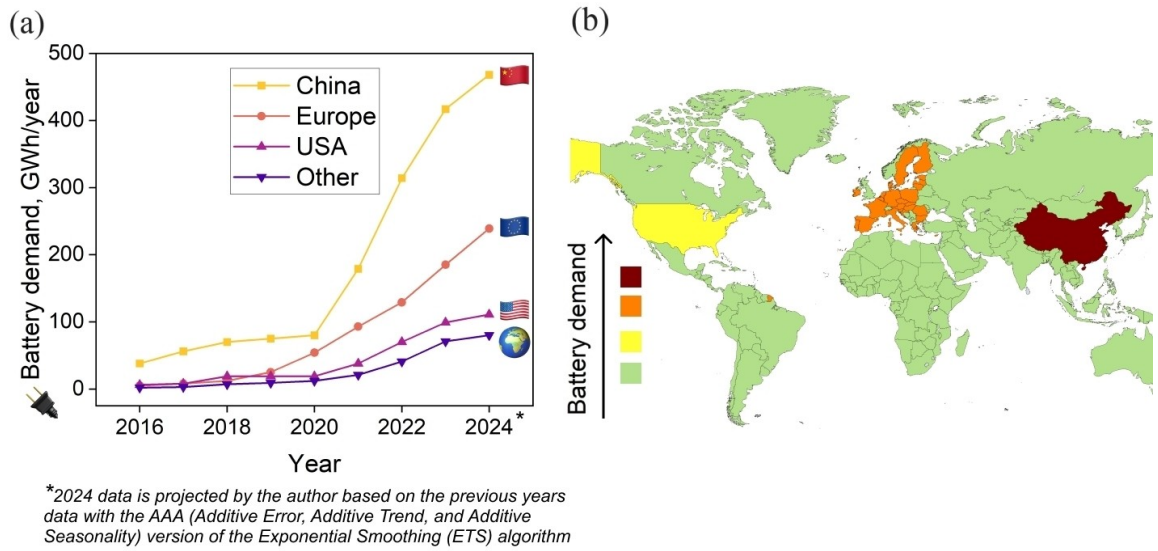

Figure 2. Trends in electric vehicle batteries: global Li-ion battery demand from 2016 to 2024 (a) per year and (b) map distribution in 2023 according to the International Energy Agency (IEA).

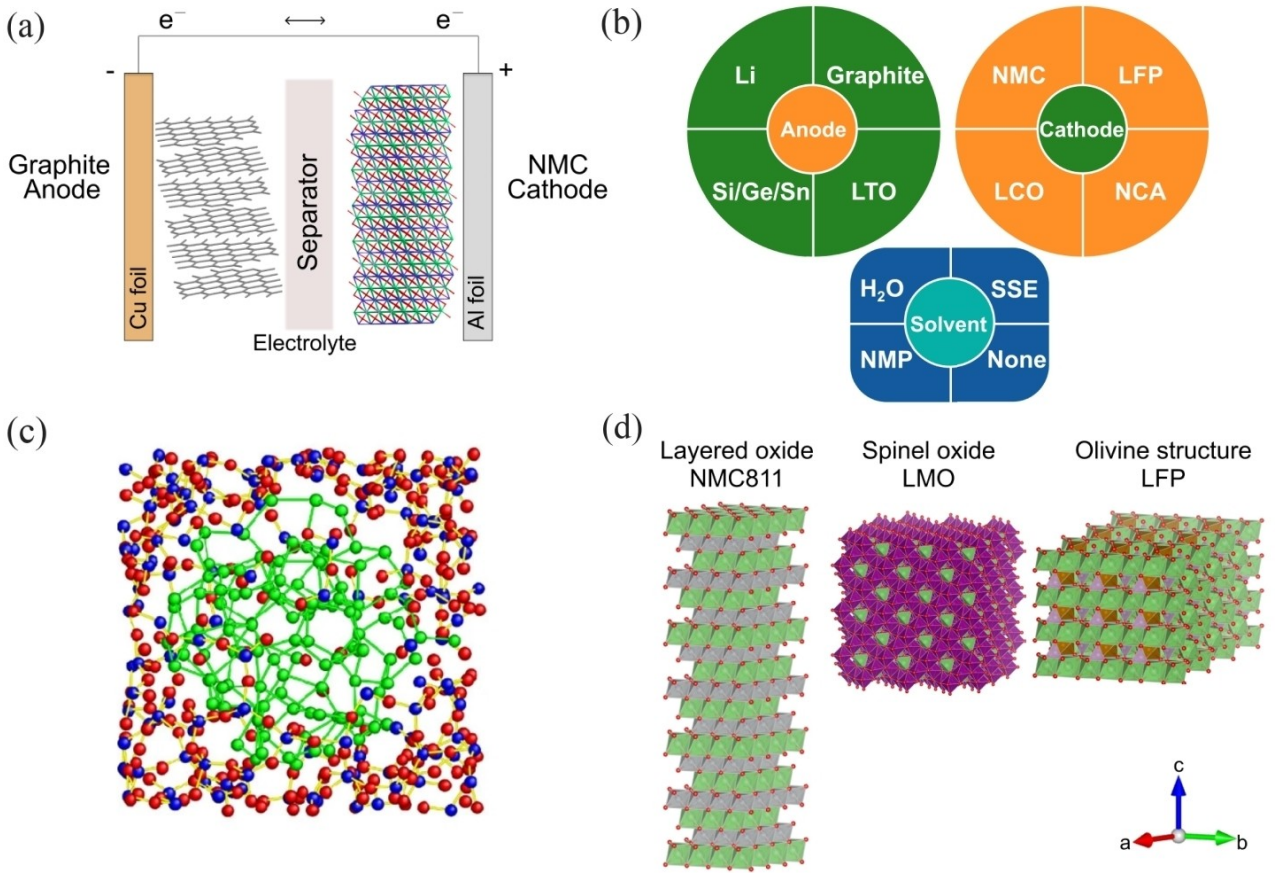

Figure 3. (a) Composition of LIB and (b) common types of materials and solvents. (c) Reconstructed heterostructure model of amorphous SiO. The inner part corresponds to an amorphous Si cluster and the outer part is amorphous SiO_2 matrix. The blue, red and green circles denote Si and O in amorphous SiO_2 and Si in the Si cluster, respectively.[21] (d) Crystal structure of typical cathode materials for LIBs: layered oxide NMC811, spinel oxide LMO, and olivine structure LFP.

offer good cycling performance, allowing the battery to endure numerous charge and discharge cycles.[6] The morphology of the graphite significantly impacts its performance; for instance, spherical graphite enhances packing density, thereby improving the overall energy density of the battery.[7] Artificial graphite, with its higher performance compared to natural graphite, is a

preferred choice for industries aiming to optimize battery technologies.[8] Artificial graphite can be engineered have high purity and specific crystal structures. In contrast, natural graphite is simpler to mine, making it more cost-effective. However, both natural and artificial graphite anodes are limited by a theoretical capacity of 372 mAh g^{-1}. Additionally, the formation and growth of the solid electrolyte interphase (SEI) layer present challenges for these anodes. Hard carbon is an alternative anode material for lithium-ion batteries, exhibiting specific capacities greater than 400 mAh g^{-1}.[9–11] Current research is focused on overcoming issues with cycling stability and manufacturing complexity to further improve hard carbon anode performance.

Lithium metal, with its high theoretical capacity of 3860 mAh g^{-1} and low redox potential (−3.04 V vs. standard hydrogen electrode), is a promising anode material.[12–14] However, dendrite growth during charge and discharge cycles leads to the formation of "dead lithium," deterioration of the SEI film, and reduced Coulombic efficiency (CE). Significant volume changes during cycling also pose practical challenges. Optimizing electrolyte formulations, particularly with additives (< 5% by volume or weight), can suppress dendrite growth and regulate $Li+$ ion deposition, enhancing cell performance.[15–18] Solid-state electrolytes also show promise in suppressing dendrite formation and enabling higher energy densities, making their investigation crucial for advancing lithium metal batteries. Computational modeling and simulation can accelerate development by predicting anode behavior and optimizing electrolyte compositions.

Silicon-based anode materials are being extensively researched due to their affordability and high theoretical capacity of 3579 mAh g^{-1}, nearly ten times that of graphite. Strategies to facilitate their use include synthesizing silicon as periodic nanostructures or nanoparticles and creating silicon-carbon composites with core-shell structures (Figure 3 (c)). Non-stoichiometric SiO_x ($0 < x < 2$) is particularly promising for high-capacity lithium-ion anodes.[19] SiO_x is an amorphous material, often a two-phase mixture of silicon and silicon dioxide nanodomains.[20] The formation of lithium oxide and silicates provides buffer zones that mitigate volumetric changes during (de)lithiation, resulting in significantly higher cycling stability compared to pure silicon.

Germanium (Ge) and tin (Sn) are also strong candidates for anode materials due to their high theoretical capacities (1600 mAh g^{-1} and 984 mAh g^{-1}, respectively).[22] Germanium boasts 400 times faster lithium-ion conductivity and 104 times higher electrical conductivity than silicon.[23] However, challenges such as volume expansion, mechanical degradation, and the formation of unstable SEI layers remain.

$Li_4Ti_5O_{12}$ (LTO) is a spinel material and a promising anode for lithium-ion batteries, known for its commendable cycle stability, rate capability, and safety. Despite zero volume change during charge and discharge cycles, its theoretical capacity of 175 mAh g^{-1} is insufficient for grid-scale energy storage and electric vehicles (EVs).[24,25] Additionally, LTO production costs are generally higher than those of some other anode materials. Continued research to improve performance and reduce production costs is essential for positioning LTO as the future of energy storage solutions.

2.2. Cathode

Different oxides and phosphates are the most popular types of cathode materials (Figure 3d), each offering unique advantages and limitations, making them suitable for various applications and performance requirements.

Layered oxides ($LiMO_2$, M═Ni, Co, Mn) are commonly used as cathode materials in LIBs due to their favorable electrochemical properties. $LiCoO_2$, first commercialized by Sony Corporation in the 1990s, plays a pivotal role in the history of LIBs. This material exhibits a high theoretical specific capacity of over 270 mA/g, a relatively high operating potential (> 3.6 V vs. Li), and adequate cycle life.[26] However, it also has limitations, such as thermal stability issues and the high cost of cobalt, which is environmentally damaging to extract. Currently, NMC-type ($LiNi_{1-x-y}CO_xMn_yO_2$) cathodes dominate the market, particularly those with reduced cobalt content, ranging from NMC532 to NMC811.[27] Increased nickel concentration enhances specific capacity, rising from 160 mAh g^{-1} in NMC111 to 200 mAh g^{-1} in NMC811.[28] NCA ($LiNi_{1-x-y}Co_xAl_yO_2$) cathodes typically have a higher nickel content compared to NMC cathodes, offer improved specific capacity and high energy density, making them suitable for high energy storage applications such as EVs.

Spinel oxides (LiM_2O_4, M═Mn, Ni) are another paramount class of cathode materials in LIBs. They are less expensive and more environmentally friendly compared to other cathode oxides. The three-dimensional ion arrangement in spinel structures offers advantageous characteristics for electrochemical energy storage. LMO ($LiMn_2O_4$) is the most studied spinel oxide and has entered the EV market. However, its low capacity, energy density, and short lifetime due to structural instabilities during cycling limit its use. Ni-doped spinel oxide ($LiNi_{0.5}Mn_{1.5}O_4$) is promising due to its strong cycling characteristics and relatively large capacity, with a dominant peak at 4.75 V.[29] Despite using a more expensive component (nickel), the increased energy density reduces material costs per kWh.

Olivine structures ($LiMPO_4$, M═Fe) have attracted significant interest as cathode materials due to their high theoretical capacities and redox potentials (3.45 V vs. Li for $LiFePO_4$). However, issues such as poor electronic conductivity and slow lithium-ion diffusion need to be addressed. Current developments focus on overcoming these drawbacks through surface modification approaches like carbon coating[30] and doping with conductive materials.[31] Enhancing the specific capacity and rate capability of olivine cathodes through heteroatom doping and alloying with transition metals has shown promising results. Although $LiFePO_4$ (LFP) has lower energy density compared to $LiCoO_2$, it compensates with better safety characteristics. Thus, olivine-structured materials present an effective alternative for LIB cathodes.

Overall, each type of cathode material, from established ones like lithium cobalt oxide ($LiCoO_2$) to emerging candidates like olivine-structured lithium iron phosphate ($LiFePO_4$), has

distinct advantages and disadvantages. Transition metal oxides like $LiCoO_2$ and nickel manganese cobalt oxide (NMC) are ideal for applications requiring small, lightweight battery systems due to their high specific capacities and energy densities. However, concerns regarding cost, resource availability, and safety, especially related to cobalt supplies, have driven research into alternative compositions. Advanced characterization techniques and computer simulations have expanded our understanding of cathode materials. Future studies will likely focus on more affordable and sustainable options, achieving higher energy and power densities, and addressing critical issues such as resource shortages, environmental impacts, and safety concerns. The battery research community has the opportunity to unlock the full potential of cathode materials, ushering in a new era of advanced energy storage solutions.

2.3. Solvent

The components of LIB slurries include a combination of solvent-dispersed electrolytes, binders (*e.g.*, polyvinylidene fluoride, or PVDF), conductive additives (*e.g.*, carbon black or graphite), and active materials (*e.g.*, lithium compounds). Solvents are crucial, despite often being taken for granted. They dissolve electrolytes, binders, and conductive additives to create homogeneous slurries, which are then deposited onto electrode substrates to form the active material layers inside the battery. The solvent choice significantly influences the morphology, porosity, and adherence of electrode coatings, as well as the rheological characteristics of the slurry, thereby affecting the performance, stability, and safety of the battery.

N-Methyl-2-pyrrolidone (NMP) is a widely used polar aprotic solvent in the fabrication of cathodes and some types of anodes for LIBs. NMP dissolves binders like PVDF, promoting good wetting of electrode materials, ensuring proper adhesion, and uniform distribution of active materials on the current collector, which is essential for maximizing the electrochemical performance and stability of LIBs. However, NMP is classified as a reproductive toxicant and poses health and safety risks, especially with improper handling or prolonged exposure. Due to potential health and environmental concerns, there is significant interest in finding NMP substitutes. Alternatives like ionic liquids, deep eutectic solvents, and supercooling solvents are being investigated for their lower environmental impact.[32–34]

Water-based slurries offer a viable alternative to conventional organic solvent-based slurries, particularly favored for anode preparation, as some anode materials like silicon are incompatible with NMP. For instance, water has been proposed as a substitute for NMP in electrode fabrication and black mass recovery during battery recycling in green manufacturing and direct recycling approaches. Electrochemical performance of water-processed electrodes has been shown to be equivalent to that of NMP-based electrodes.[35] Wood et al.[36] reported that switching from NMP to water-based solvents could reduce battery pack costs by 2% and save $3–6 million in capital investment.

Dry processing technologies have emerged as a viable option, offering several advantages over conventional wet processes, including reduced energy consumption and elimination of safety issues related to flammable solvents. Dry processing methods, such as thermal evaporation, sputtering, powder pressing, and dry mixing, reduce or eliminate the need for liquid solvents in battery manufacturing. For example, Wang et al.[38] studied the effects of high-speed and ball mill mixing prior to electrostatic spray deposition (ESD) on dry-made electrodes. These techniques often require lower energy inputs than wet processes since they do not involve solvent evaporation or drying stages. In particular, the energy requirement for manufacturing with NMP is high, at 10.2 kWh per kilogram of vaporized NMP and 421 kWh per 10 kWh battery pack, with the total energy requirement being 45 times the heat required for NMP vaporization.[37]

In summary, exploring LIB solvents is crucial for improving the efficiency, safety, and sustainability of energy storage technologies. Through extensive research and innovation, a variety of solvent solutions have been identified, ranging from traditional organic solvents to water-based alternatives. This ongoing investigation holds promise for advancing the performance and environmental compatibility of lithium-ion batteries.

3. Device and System Manufacturing and Production

3.1. Cell Types and Battery Manufacturing Line

To produce high-quality battery cells or packs, a lithium-ion battery (LIB) production line typically comprises numerous interrelated processes and stages (Figure 4a). The cell and battery casing types of LIBs can vary based on several parameters, including application, size, performance requirements, and safety concerns. The most common materials for casings are aluminum, plastic, and stainless steel. Typical designs for LIB cells include:

(1) Coin Cells: Small with high energy density, these are often used in small electronic devices. Named for their coin-like appearance, they can be identified by standard sizes such as CR2032 or CR2025.
(2) Pouch Cells: Flexible, thin, and lightweight, these are widely used in devices like computers, tablets, smartphones, e-bikes, and electric scooters. Pouch cells are economical to manufacture and offer a high degree of design flexibility.
(3) Cylindrical Cells: Known for their high energy density and durability, these cells have a tubular shape that simplifies loading and stacking in battery packs. They are commonly found in large-scale energy storage systems, electric vehicles (EVs), and consumer electronics.

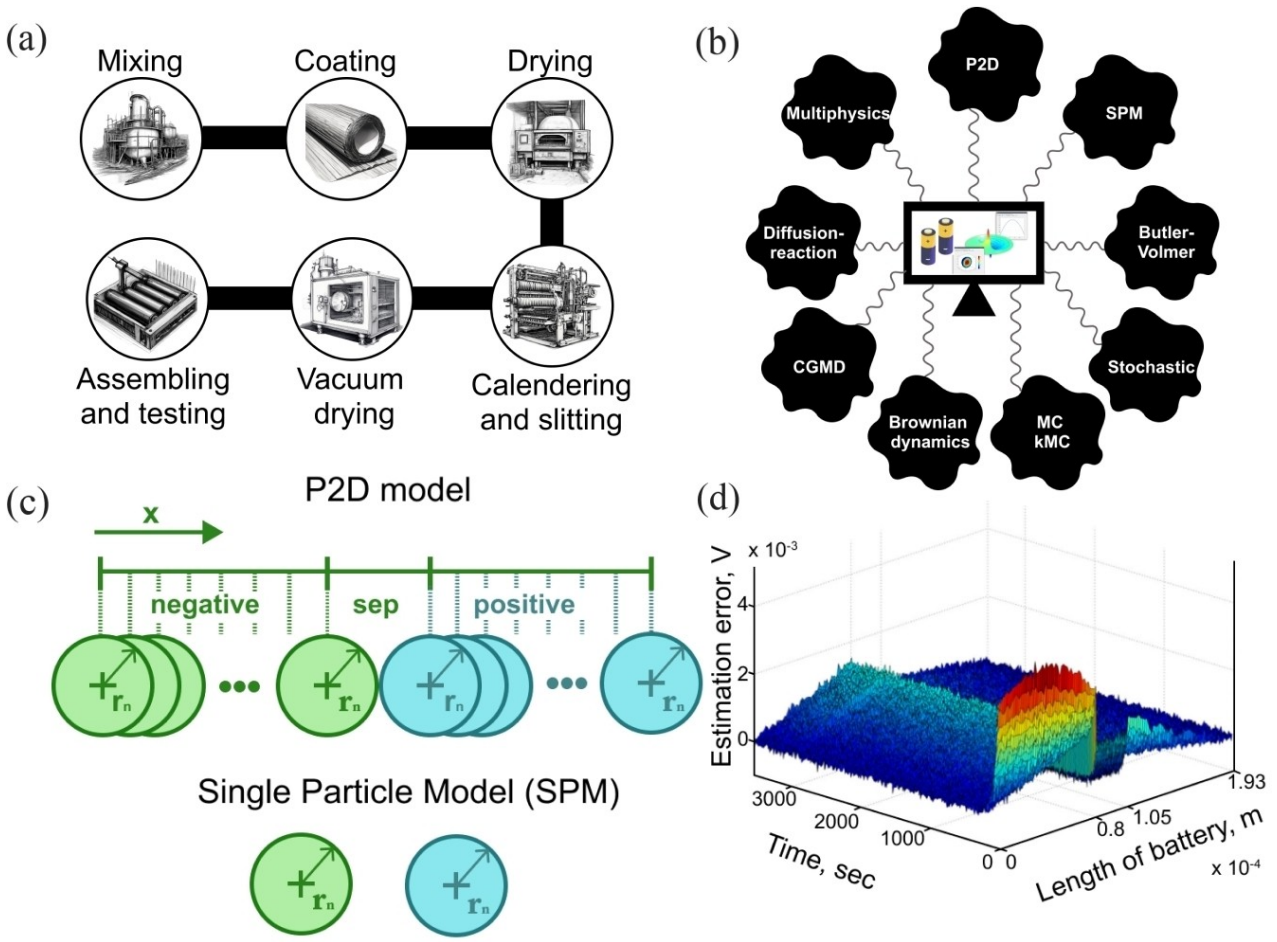

Figure 4. (a) Diagram of the production stages for LIBs. (b) Diversity of physical and mathematical modeling techniques for advanced battery manufacturing. (c) Model structure for P2D and SPM Li-ion cell.[41] (d) Electrical potential in electrolyte estimation via stochastic P2D modeling.[43]

(4) Prismatic Cells: With a rectangular shape, these cells are easy to stack in battery packs and are used in various applications, including energy storage systems and EVs.

Various models from fields such as chemistry, physics, and artificial intelligence (AI) are employed in the development and manufacturing of LIBs to enhance productivity, ensure high-quality battery products, and optimize processes. These models are categorized into physics-based, AI and machine learning, and data-driven models. This review will discuss both cell and battery pack levels.

3.2. Cells: Intelligent Equipment and Smart Manufacturing

3.2.1. Physical and Mathematical Modeling

Physics-based models and their mathematical representations (Table 1) are critical for creating intelligent materials and devices for LIBs. These models (Figures 4b, 6) mimic and forecast different processes in battery cells and manufacturing equipment using the principles of physics. If manufacturers incorporate physics-based models into the design, quality, and operation of their manufacturing processes, they may enhance performance, quality, and sustainability throughout the whole Li-ion battery production chain.

Complex lithium-ion diffusion mechanisms and the corresponding electrochemical reactions in electrode materials are crucial for LIB applications. Diffusion-reaction models are valuable for elucidating these fundamental mechanisms and improving battery performance. Fick's diffusion equations govern the flow of lithium ions between the cathode and anode in an LIB. These equations describe the diffusion of lithium ions through complex electrolytes driven by concentration gradients, with the material's diffusion coefficient influencing the diffusion rate. This process can be mathematically represented as a partial differential equation, where the concentration of lithium ions is dependent on both time and space:

$$\frac{\partial c}{\partial t} = D\nabla^2 c \tag{1}$$

where c represents the lithium concentration, t denotes time, and D is the diffusion coefficient. Zhang et al.[39] proposed a new reaction-controlled diffusion model with the help of the bond-breaking energy barrier E_0 as the key physical quantity.

Table 1. Key discussed techniques for mathematical and physical modeling.

Model	Application
Diffusion-reaction[39]	Description of diffusion mechanisms and corresponding electrochemical reactions in electrode materials
Butler-Volmer[40]	Investigation of the relationship between an electrode's current flow and the potential differential across it. The battery performance modeling and the charge transfer kinetics at both electrode surfaces
P2D[41–44]	Study of battery activity and internal electrochemical processes, including each layer
SPM[44,46]	Beneficial through the easy parameter estimation process and the representation of each individual particle
Multiphysics[47–67]	Insights into battery behavior throughout various operating scenarios. Design, development, and management of contemporary battery systems by integrating several factors
Stochastic[68–74]	Understanding the relationship between microstructure and characteristics of batteries
MC and kMC[75–80]	Resemblance of unpredictable natural systems. Study of lithium plating and insertion kinetics under various scenarios
Brownian dynamics[81–85]	Analysis of every electrode slurry characteristic and the process of aggregation
CGMD[85–88]	Ion diffusion and transmission modeling, evaluating the drying process for electrodes

This model may offer several approaches to enhancing the performance of Si by enhancing the diffusion property between Li and Si or the speed of the chemical reaction by handling diffusion and reaction independently. In other materials, like germanium, this model may also be able to describe the complex phase transition caused by diffusion.

Another key method is the Butler-Volmer (BV) equation, derived from the principles of thermodynamics. This electrochemical equation describes the relationship between the potential difference across an electrode and the current flowing through it. The BV equation is also used in simulating battery performance and the kinetics of charge transfer at both cathode and anode interfaces during charging and discharging. Lu and colleagues proposed a modified version of the Butler-Volmer equation to account for the impact of mechanical stresses on electrochemical processes in lithium-ion battery electrodes.[40] They discovered that compressive stress in the active material's surface layer impedes lithium intercalation, requiring an additional electrical overpotential to overcome the stress-induced reaction barrier. The modified equation, incorporating stress effects, was first identified as:

$$i = i_0 \left\{ exp\left[(1-\alpha) \frac{F\left(E_v - E_{eq}\right) - \sigma_h \Omega}{R_g T} \right] - exp\left[-\alpha \frac{F\left(E_v - E_{eq}\right) - \sigma_h \Omega}{R_g T} \right] \right\} \quad (2)$$

where i_0 is the exchange current density, R_g is the universal gas constant, T is the temperature, and α is the charge transfer coefficient, σ_h is the hydrostatic stress and Ω is the partial molar volume, F is the Faraday constant, E_v and E_{eq} are the electrode potentials at the present state and at the chemical equilibrium state, respectively.

Under both open-circuit and galvanostatic operating circumstances, the model has demonstrated a linear relationship between the voltage hysteresis height and the hydrostatic stress differential between lithiation and delithiation. The theoretical models predicting the electrical overpotential for thin-film silicon electrodes align well with practical evidence.

A frequently used technique in the modeling of LIBs is the pseudo-two-dimensional (P2D) model (Figure 4c). This model strikes a balance between accuracy and computational complexity, making it a superior option for studying battery activity. The battery is represented as a stack of pseudo-two-dimensional layers, allowing for a comprehensive description of electrochemical processes within. Solving a P2D model for LIBs often requires numerically solving coupled differential equations that depict the various physical processes occurring inside the battery. As this is computationally intensive, it is unsuitable for real-time control applications.[41] The model accounts for several transport processes within each layer, including electron transport through the electrodes and lithium-ion diffusion within the solid electrode materials and electrolyte. The kinetics of charge transfer during charge and discharge cycles are described by the Butler-Volmer equation, which also considers mechanical variables. Recently, Laue et al. showed that a three-step procedure combining the classical C-rate test with OCP measurements is insufficient for P2D model identification.[42] In quasi-static settings, highly dynamic tests (such as impedance spectroscopy) are needed to clarify the ambiguity of diffusive and electric processes. A mix of quasi-static and highly dynamic testing, along with experimental data from electrode-resolved experiments, is required for any parameterization of electrochemical models. Utilizing the P2D model, Tulsyan et al.[43] introduced a novel approach for state-of-charge estimation. It was proved that reducing computing complexity by using an unusual strategy called "tethering," yielding precise state-of-charge estimates. This method could potentially be adapted to include state-of-health equations. The predictive ability of a parametrized Doyle-Fuller-Newman (DFN) model was demonstrated using a commercial cylindrical (21700 cell) Li-ion cell with an NCA cathode and a Gr-SiO_x anode.[44] The cell voltage was predicted using the DFN model in two scenarios: (i) a driving cycle with a highly non-uniform current distribution and (ii) a constant current discharge under varying discharge rates.

Compared to the computationally expensive P2D model, the single-particle model (SPM) offers an attractive alternative for several applications. The SPM simplifies battery representation by modeling each electrode particle as a single entity while retaining key battery features. This approach, developed from

comprehensive electrochemical models, involves a limited set of ordinary differential equations, reducing the risk of overfitting and simplifying parameter estimation. Guo et al. extended the SPM to include thermal effects and added an energy balance equation.[45] They solved the solid-phase diffusion equations using the eigenfunction expansion approach instead of a two-term polynomial approximation, increasing the model's accuracy. Identifying primary stress elements is crucial for constructing an appropriate model. For instance, concentration polarization must be included, as the system is significantly affected by temperature and current.[46] Consequently, with a constant current of ±0.5 C/1 C and a SOC of 2%–98%, the compensated model's error is within ±40 mv.

Integrating several physical processes that happen within the battery at the same time is the complex topic of multiphysics modeling of LIBs.[47–52] The term "multiphysics" in the literature often refers to models that theoretically explain interactions between mechanisms from several physical domains.[53] Most models designed to explain LIB function fall into this category as they must consider at least two distinct physical domains: charge transfer and electrochemistry. Multiphysics models provide critical insights into battery behavior under various operating conditions, aiding the design, development, and management of modern battery systems by combining electrochemical, thermal, mechanical, and transport processes. The first publication on coupled mechanical-electrical-thermal simulation of battery failure at the cell level was introduced in 2015 (Figure 5a).[54]

Using a representative-sandwich finite-element model in the commercial program LS-DYNA©, the combined mechanical-electrical-thermal response was simulated. Each component, such as the active material, current collector, and separator, was explicitly represented, predicting their mechanical deformation under quasi-static indentation. The stress-strain relationship was calculated as follows:

$$\sigma = \int_0^{\varepsilon} E d\varepsilon = \begin{cases} \frac{E_{max}\left(e^{\beta\varepsilon}-1\right)}{\beta e^{\beta\varepsilon_p}} & \varepsilon < \varepsilon_p \\ \frac{E_{max}\left(1-e^{-\beta\varepsilon_p}\right)}{\beta} + E_{max}\left(\varepsilon - e_p\right) & \varepsilon \geq \varepsilon_p \end{cases} \quad (3)$$

where E denotes the Young's modulus, E_{max} represents a fully compacted value modulus, ε is the strain, ε_p corresponds to the strain when the material is fully compacted and β is the fitting parameter.

The first cells based on $Li_xNi_{1/3}Mn_{1/3}Co_{1/3}O_2$ were described by Smekens et al.,[55] demonstrating good consistency with actual data, except for some issues with voltage drop prediction at high current rates. Additionally, it was determined that the porous electrode model can qualitatively simulate electrodes made of graphite or NMC. Other materials characterized using multiphysics models included carbon fiber,[56] hard carbon,[57] silicon,[58,59] and Si/graphite composites.[60,61] Using the COMSOL software, a pseudo-mesoscale finite element model with a Ni-rich layered oxide (NMC622) cathode was developed.[62] The diffusion of lithium was modeled using Fick's law, while the kinetics of electrochemical reactions were represented by the Butler-Volmer equation. It is important to note that, because half-cells had an infinite supply of Li-ions, boundary conditions were primarily applied to the cathode.

Several research groups have shown interest in multiphysics modeling of separators for LIBs.[63–65] Wu et al.[66] conducted the first in situ evaluation of stresses in a PP separator using a multiphysics model. By coupling the time-temperature superposition principle (TTSP) with thermo-viscoelastic modeling, they characterized the PP separator. The physics-based model

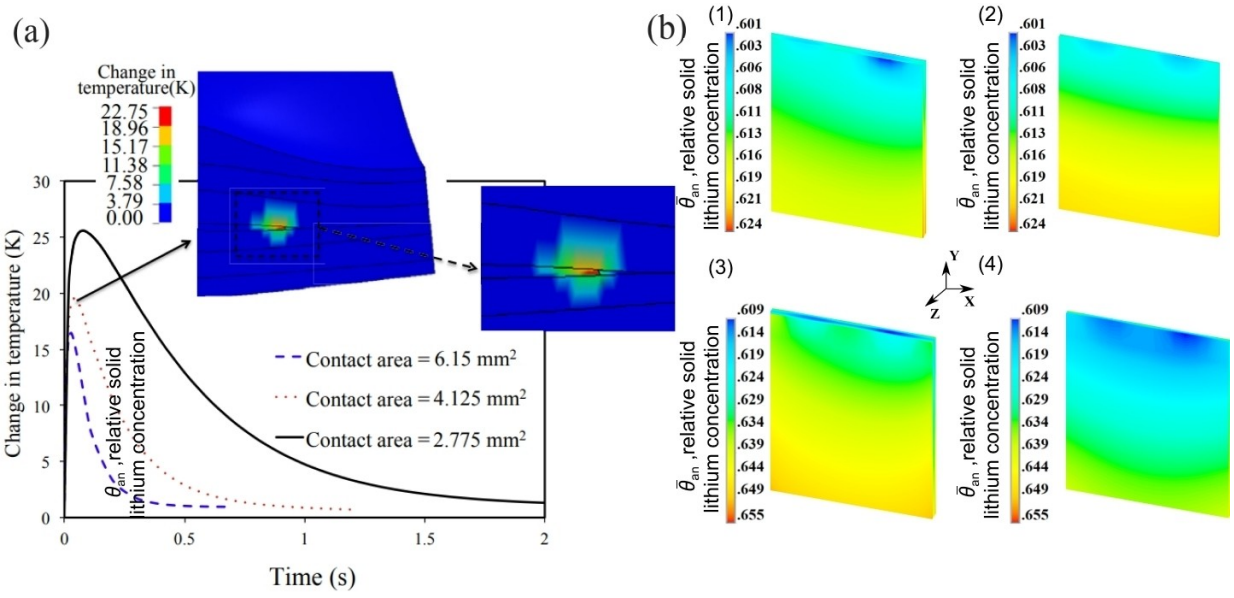

Figure 5. (a) Coupled thermal-electric response of a mechanically crushed pouch cell: highest increase in local temperature across the short-circuit following an indentation-induced short-circuit for various electrical contact areas in a 740 mAh LIB.[54] (b) Multiphysics modeling of relative solid lithium concentration on anode surface at SOC = 50%: at 1 C in (1) surface and (2) central layers, at 4 C in (3) surface and (4) central layers.[67]

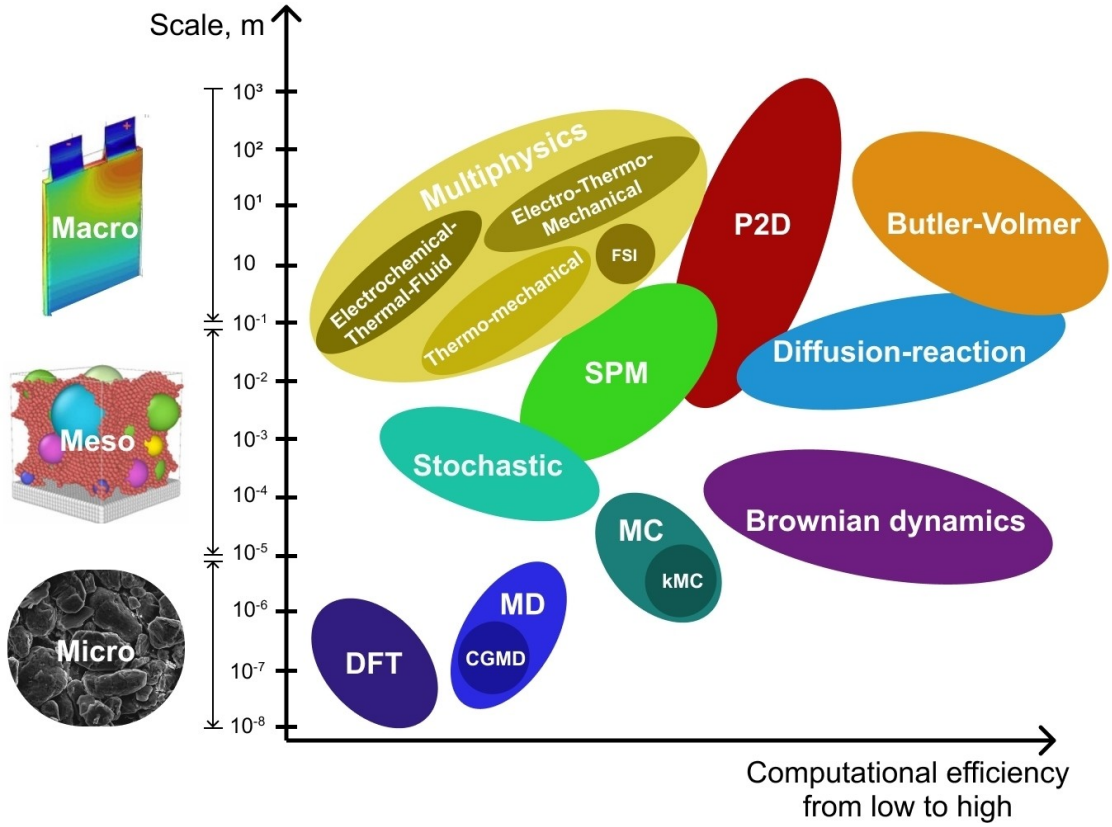

Figure 6. Relationship between scale (micro, meso, macro) and computational efficiency (from low to high) of discussed physical/mathematical models.

comprises four sub-models, *i.e.*, Battery, Electrode, Thermal, and Stress. The overall strain across the cell is the sum of three types of deformations:

$$\varepsilon_{ij} = \varepsilon_{ij}^{me} + \varepsilon_{ij}^{ei_T} + \varepsilon_{ij}^{ei_c} \quad (4)$$

where ε_{ij}^{me} denotes the strain due to mechanical loading, and $\varepsilon_{ij}^{ei\_T}$ and $\varepsilon_{ij}^{ei\_c}$ denote the eigen strain due to thermal expansion and Li intercalation, respectively.

To study detailed multiphysics heterogeneity in multiple layers of a 12 Ah large-format pouch cell at varying discharge rates, a new 3D multiphysics model with excellent computing efficiency was created (Figure 5b).[67] The framework consists of two levels: electrode submodels and cell submodels. Validation of the reduced electrochemical submodel was performed up to a 4 C discharge rate using a P2D model. It was determined that while cell temperature is uniformly distributed at low discharge C-rates, cell performance is significantly impacted by thermal behavior at high discharge C-rates. At low C-rates, the electrostatic potential predominantly influences the local current density at the current collectors. Therefore, local current density and temperature factors interact with electrochemical performance at high C-rates.

Stochastic (random) modeling, which involves representing battery behavior using mathematical equations, is a highly effective and versatile technique for creating both anode and cathode structures.[68–70] Stochastic modeling incorporates variability by expressing uncertain parameters as random variables that correspond to certain probability distributions. Understanding the relationship between battery microstructure and characteristics benefits greatly from 3D electrode morphology. For complex, nonlinear systems, advanced approaches like Markov Chain Monte Carlo (MCMC) methods[71] and Bayesian inference[72] can be used to estimate parameters more accurately. Thiedmann et al.[72] created a 3D stochastic simulation model of composite materials based on stochastic geometry and spatial statistics. Stochastic modeling has also been applied to plug-in hybrid electric vehicles,[73,74] for example, the capacity loss and usage time of LIBs with NMC–LMO chemistry were predicted.[73] Using the Gaussian distribution and computing the mean and standard deviation of error, the stochastic component of the capacity fade model yields a mean to characterize the fluctuation of the capacity and resistance relationship. The general model for stochastic life prediction is given by:

$$Q_{pred} = Q_{ratio}(R_{syn}) + \omega \quad (5)$$

where ω, or $\omega \sim N(\mu, \sigma^2)$, is the random term with a normal distribution.

Applications for Monte Carlo (MC) and Kinetic Monte Carlo (kMC) have also been identified in LIB manufacturing. These methods work by executing large quantities of random operations to produce outcomes that resemble inherently

unpredictable natural systems.[75] A kMC simulation requires a collection of discrete configurations and prior knowledge of a set of transition rate constants describing the transition events between these configurations. Several electrochemical models of lithium plating have been developed under various operational scenarios.[76,77] It is well-known that lithium plating is a primary cause of capacity decline and safety issues in lithium-ion batteries. Zhang et al.[76] demonstrated that rapid charging rates, low temperatures, high states of charge, and high starting concentrations of Li^+ enhance the probability of Li plating. Furthermore, kMC has been frequently employed in research on the kinetics of Li-ion insertion in graphite electrodes.[78–80] These simulations provide atomistic information on the phenomena, making them valuable tools for explaining the electrochemical behavior of Li + insertion. For example, a unique strategy based on a model was adopted, which uses process models to explain the electrode manufacturing process and a physical-based battery cell simulation to examine the final result. By connecting the two model sections via transferred structural parameters, different parameter levels can be coherently considered, allowing for the study of uncertainty propagation from the manufacturing process to the performance of the LIBs.

Brownian dynamics is the most elementary type of stochastic dynamics, characterized by a lack of spatial or temporal correlations.[81] Stochastic differential equations, including the simplified Langevin equation, help us understand Brownian dynamics by indicating the limit where there is no average acceleration. Ermak and McCammon developed a technique in 1978 for modeling the Brownian dynamics of *N* particles with the addition of hydrodynamic interactions, nearly 50 years ago.[82] The aggregation process between LMO and carbon black (CB) was simulated using Brownian dynamics, and the Langevin equation was used to control the particle trajectory.[83] Regarding anodes, dilute suspensions composed of silicon and carboxymethylcellulose sodium salt (CMC) were analyzed using Brownian dynamics simulations with a coarse-grained model.[84] Using a 3D coarse-grained Brownian dynamics model, the impact of the Damköhler number on morphology and lithium deposition under an applied voltage was investigated.[85] Research has demonstrated that rapid kinetics promote dendritic development, whereas slower kinetic deposition leads to significantly more uniform, dense, and compact deposition.

The coarse-grained molecular dynamics (CGMD) modeling mesoscopic approach is primarily used to analyze the behavior of large molecular systems, such as proteins[85] and nucleic acids.[86] This method reduces computational costs by representing groups of atoms as single particles with fewer degrees of freedom. In the context of batteries, Li et al.[87] employed the CGMD simulation approach to model the working ion diffusion and transmission mechanism in the cathode of lithium-oxygen batteries. Additionally, the drying process of electrodes made from water-based suspensions was studied using CGMD simulations to predict and analyze debonding phenomena and microstructure progression.[88] It was discovered that the water-based electrode did not bind active material-active material (AM-AM) and active material-current collector (AM-CC) as effectively as NMP-based electrodes during the drying process. The ultimate volume of the water-based coating was lower than that of the NMP-based coating, leading to a more compact AM distribution after drying, which increased energy density.

3.2.2. AI-Based Modeling

Over the past several years, AI-based modeling (Table 2) has emerged as a revolutionary technique in the realm in LIB manufacturing. AI technologies (Figure 9) employ advanced algorithms and machine learning techniques to process large datasets and forecast outcomes, thereby enhancing the efficiency and productivity of battery production. For material optimization, this approach is particularly beneficial due to its ability to process vast amounts of data simultaneously while also predicting different scenarios. By utilizing data from sensors and production equipment, AI algorithms can detect inefficiencies and optimize various parameters (e.g., temperature,[89] SOC,[90,91] SOH[90,92]) in real-time, leading to significant improvements in production processes. Through the analysis of historical data and continuous monitoring of equipment performance, AI algorithms can predict potential failures and reduce periods of inactivity. Moreover, substituting manual check-ups with AI not only improves speed but also minimizes human error. Overall, enabling manufacturers to optimize processes, adjust material ratios, and enhance quality control, AI-based modeling paves the way for a new era of efficient and high-yield manufacturing of high-energy density batteries.

Inspired by the structure of the human brain, neural networks (NNs) are a key component of artificial intelligence algorithms and offer solutions for various battery challenges, including process optimization, quality assurance, and predicting battery lifespan. Layers in NNs can be categorized as input, output, or hidden layers (Figure 7a). NNs learn to organize input information into output predictions through repeated training cycles. Due to their computational efficiency, NNs can be implemented in real-time applications. Wu et al.[93] trained two NNs (the classifier and the calculator) using electrochemical-thermal model simulation results. They selected specific energy and power as outputs and compared the resulting data with finite element simulation estimations. In 2010, a technique for modeling and estimating the state of charge (SOC) of LIBs using the extended Kalman filter (EKF) and NNs was introduced.[94] The full charging cycle was divided into three sections: 70%, 35%, and 20% duty cycles, requiring the NN to be trained under varying charging conditions. The neurons located in the hidden layer are activated by Green functions, which are equivalent to Gaussian functions, and have the following form:

$$\varphi_i = G(\|r_k - t_i\|) = \boldsymbol{exp}\left(\frac{\|r_k - t_i\|^2}{\sigma_i^2}\right),\ i = 1, \ldots, M \tag{6}$$

Where r_k is the input vector, t_i and σ_i are the center and the standard deviations of the Gaussian function, and M is the number of neurons in the hidden layer.

Table 2. Key AI-based models and their implementations.

Model	Materials	Results
ANN[93]	NMC111, Li_xC_6	Using the results of the electrochemical-thermal model simulation, two NNs (the classifier and the calculator) were trained, and a continuous, precise Ragone plot was produced
Radial basis function NN with EKF[94]	N/A	The SOC estimator had rapid convergence and excellent accuracy
FNN and dynamical signal preprocessing[96]	NMC	The LIB voltage at various states was accurately simulated. The proposed model could serve as a viable alternative to the EEC
CNN[110]	LFP, NMC, NCA	Predictions were made on the primary processes of degradation
Auto-CNN-LSTM[112]	N/A	With an RMSE of 4.8%, the RUL of LIBs was predicted
LSTM, FNN, CNN[118]	NMC	Several models were used to predict the battery capacity; in terms of RMSE, LSTM performed better than CNN and FNN
SVM[122]	NMC111, graphite	The battery SOH was estimated with less than 3% error for 95% of all the cases
SVM[129]	N/A	Precise RUL estimation of numerous batteries at different temperatures and operating conditions concurrently was made possible by the multistage technique
LSSVM[125]	NMC	In SOC prediction, the model demonstrated excellent resilience and accuracy, with an error of less than 1%
PSO-SVM[134]	LFP, NCA	The online detection and estimation for the BMS were combined with the SOC-SOH joint estimation approach. SOH and SOC were predicted with an error of less than 3%
RUBoost, DT[147]	LFP, LTO	The most crucial feature variables for each electrode quality were correctly determined based on the quantified Gini significance (94.4% accuracy for LTO and 97.8% accuracy for LFP, respectively)
RF, DT, linear regression[156]	LFP, NCA, NMC	A simulated big data set was subjected to a machine learning study. For estimating the degradation modes, it was demonstrated that RFs performed better than linear regression
RFR[149]	NMC, graphite	The online battery capacity estimation method with the largest RMSE of 1.3% was developed
Bagging, boosting[161]	N/A	The prediction of the residual capacity of LIBs was performed. Research demonstrated that bagging yielded a reduced error in comparison to boosting
Gradient-boosted tree[165]	NMC, graphite	The key components were determined, along with the relative importance of each. Mass loading, capacity, and thickness - three important control parameters - were measured with a little degree of error
GLM, MLR, SPL-MLR[170]	NMC, graphite	For each SOC study example, the MLR-PSO was demonstrated to be the most successful predictor, giving the greatest overall results

Feedforward neural networks (FNNs) are the simplest form of NNs because of their uni-directional flow. Despite this simplicity, they are versatile and can be employed for various tasks, such as predicting battery properties,[95,96] estimating SOCs,[97,98] and optimizing charging and discharging processes. FNNs trained on historical data can differentiate between high-quality and subpar batteries, assisting in quality control. Additionally, they can be programmed to recognize and prevent manufacturing process flaws by detecting real-time deviations. Recently, an FNN estimator was developed to estimate the SOC of LIBs using MATLAB simulations.[99] The inputs were temperature, terminal voltage, and discharge current; the output was SOC. Prior to developing, training, and validating the FNN network, data had to be gathered and normalized. The proposed model exhibited a low mean absolute error (less than 1.5%), confirming the method's high accuracy. Dziechciaruk et al. provided a guideline for the training procedure and recommended adapting an easily estimated FNN with dynamic signal preprocessing over the traditional electrical equivalent circuit model.[96] The crucial factors included selecting appropriate training tests, the number of neurons and hidden layers, the quantity of delay filters, measurement accuracy, and sampling periods. Remarkably, the FNN was effectively trained using only three discharge tests, demonstrating that extensive data is not always necessary. Comparatively, the FNN approach outperformed the EEC model, with lower root mean squared errors in most test versions. However, significant error values at deep discharge states were observed for both models, likely due to the steep voltage profile and minor measurement errors.

Another common type of FNN is the convolutional neural network (CNN), which features a three-dimensional neuronal architecture. CNNs are particularly useful for visual recognition applications.[100–102] Regarding batteries, these neural networks have been implemented in SOC,[103] SOH,[104–106] and capacity[107–109] estimations. An accurate (2% of RMSE) and image-based method for battery degradation diagnosis was successfully presented.[110] The model's architecture comprised four types of layers: masking, convolutional, flatten, and dense (Figure 7c). Initially validated using synthetic data and later real data, the CNN model achieved an average error of 2%, significantly lower than FNN, random forest (RF), and 1D convolution models. For commercial high-power graphite/LFP systems, the model considered various degradation forms, including irreversible lithium plating, and produced superior results, opening new avenues for AI and battery research collaboration.

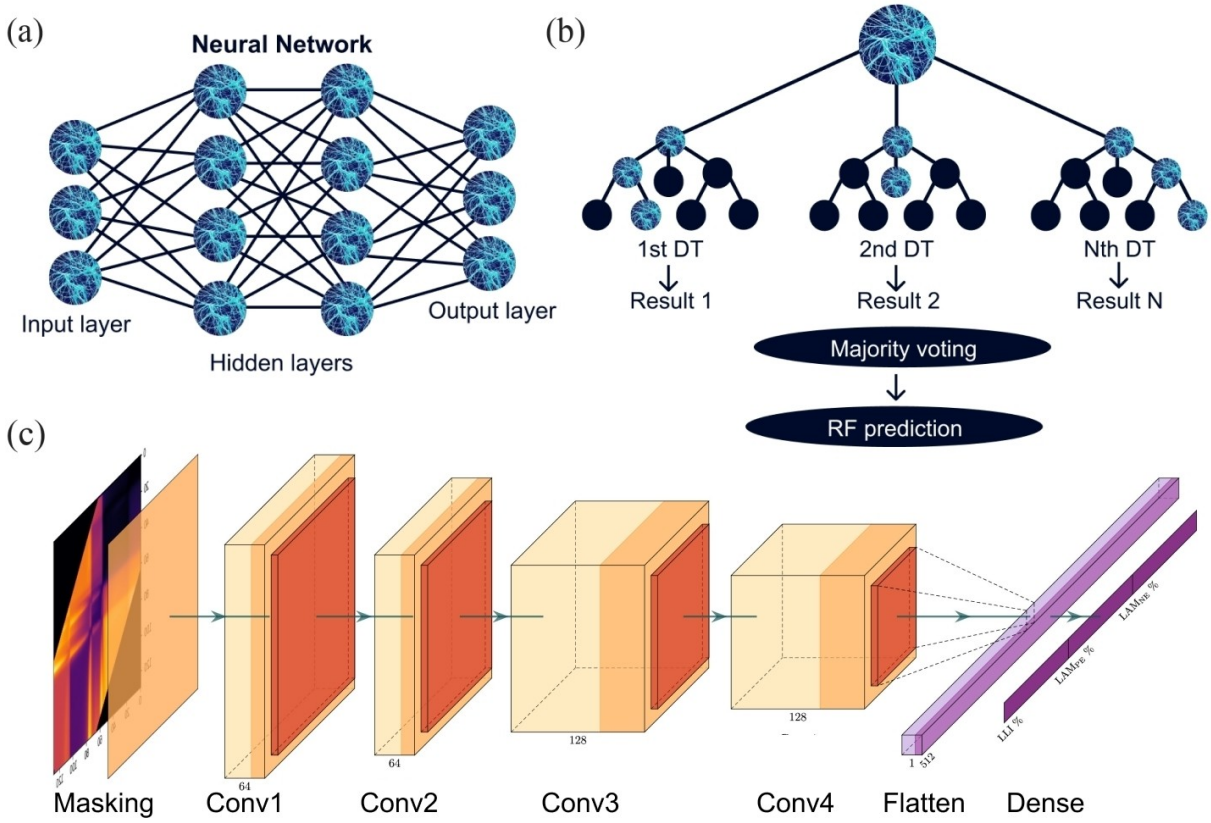

Figure 7. (a) Schematic illustration of (a) a neural network and (b) RF. (c) The suggested CNN model's structure: the max pooling layers come after the convolution layers, which are represented by Conv1 through Conv4. The three degradation models were anticipated from the condensed layer of retrieved characteristics.[110]

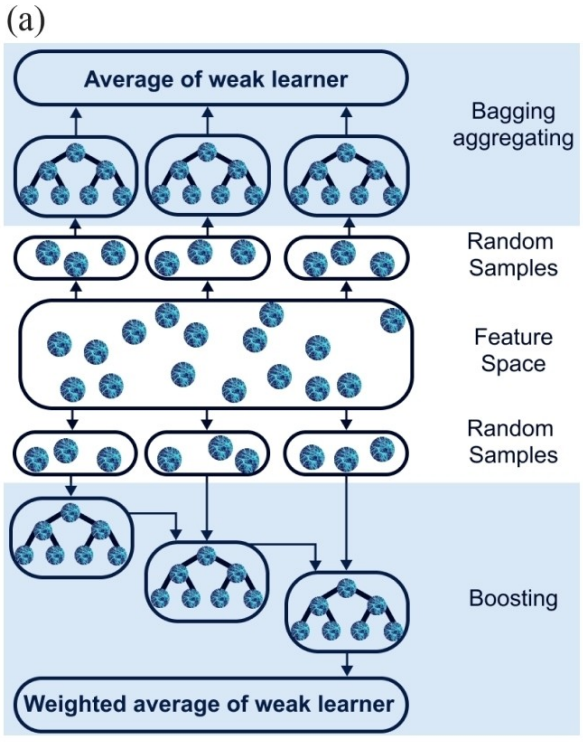

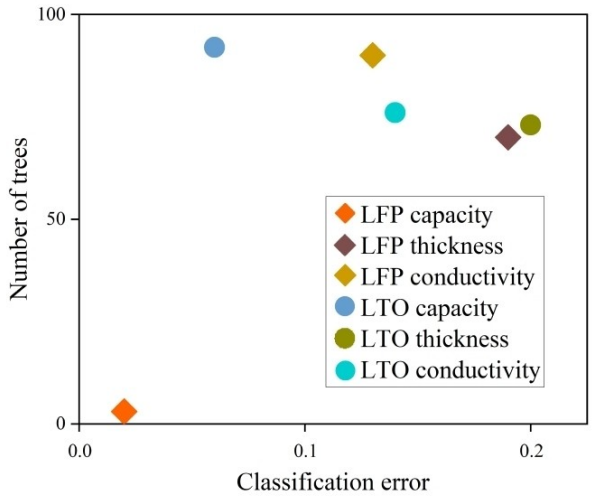

	Electronic conductivity		Thickness		Capacity	
	Error	Number of trees	Error	Number of trees	Error	Number of trees
LFP	0.13	90	0.19	70	0.02	3
LTO	0.14	76	0.2	73	0.06	92

Figure 8. (a) Illustration of bagging and boosting methods.[161] (b) Classification error and number of trees dependencies for LFP and LTO electrodes.[147]

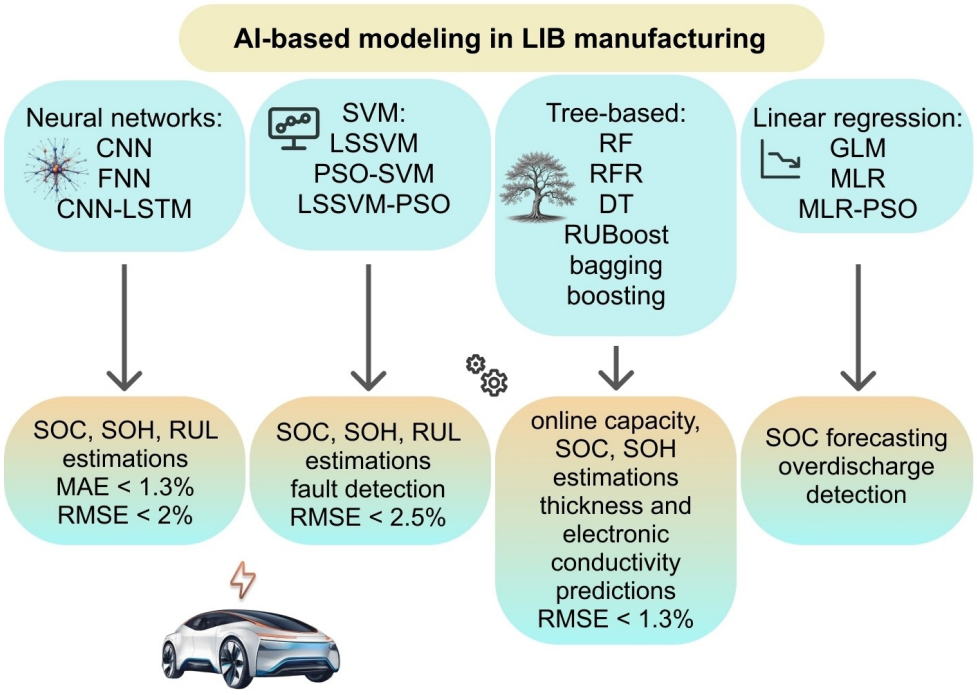

Figure 9. Key discussed AI algorithms implemented in battery manufacturing and the results of their usage with average and mean errors.

Some research groups have explored the integration of CNN and long short-term memory (CNN-LSTM) techniques.[111–115] LSTM networks are advantageous for handling data sequences by identifying long-term relationships through repeated steps. The integration of CNN and LSTM methodologies facilitates the extraction of spatial and temporal characteristics from input data. While employed similarly to CNNs, some studies have focused on estimating remaining useful life (RUL) using these hybrid networks.[112,115] For instance, Ren et al.[112] suggested an architecture (Figure 10a) where raw data from the battery is retrieved via the autoencoder. The equation for discrete two-dimensional convolution was as follows:

$$A(i,j) = \sum_{m=-s}^{s} \sum_{n=-s}^{s} K(m,n)^{*} z(i+m,\ j+n) \tag{7}$$

The following equations were implemented to determine each gate function and state transfer process in the LSTM process:

$$f^t = \sigma(W_f \cdot [h^{t-1},\ x^t] + b_f) \tag{8}$$

$$i^t = \sigma(W_i \cdot [h^{t-1},\ x^t] + b_i) \tag{9}$$

$$\overline{C^t} = \boldsymbol{tanh}\left(W_g \cdot [h^{t-1},\ x^t] + b_g\right) \tag{10}$$

$$o^t = \sigma(W_o \cdot [h^{t-1},\ x^t] + C^t) \tag{11}$$

$$C^t = f^t * C^{t-1} + i^t * \overline{C^t} \tag{12}$$

$$h^t = o^t * \boldsymbol{tanh}(C^t) \tag{13}$$

where Wstands for connection weight and b for offset parameters, C^t for the intermediate variable, which was multiplied by the input gate result and sent to the state space. Also, f was for forgetting, i for input, o for output gate outputs; h^t for t moment hidden layer output, and x^t for input at time t.

Based on the experimental findings, the RUL prediction performance of the model appears to be good, with an acceptable root mean squared error (RMSE) of 5.03%. Two factors contributed to the observed error: the influence of noise in the data and an inadequate quantity of data. The model was further compared with the Adaptive Deep Deterministic Neural Network (ADDN) model[116] (18.23% of RMSE) and the SVM model[117] (11.8% of RMSE). The accuracy of the algorithm was slightly improved by 0.19% when linear filtering was applied to enhance the data quality.

Studies comparing various neural network types have demonstrated remarkable success.[118–120] When selecting an appropriate method, the type of input data and the specific task must be considered. Feedforward neural networks (FNNs) are practical for small datasets and are relatively simple to deploy without requiring significant computational resources. Conversely, convolutional neural networks (CNNs) are adept at detecting hierarchical patterns in visualizations such as images or 2D material structures, but they require large amounts of data for effective training. Long short-term memory (LSTM) networks perform well for lengthy data sequences and can be used for forecasting time series. According to Kaur et al.,[118] LSTM outperform FNNs and CNNs in test performance evaluations if computational resources are not a constraint (Figures 10b, c).

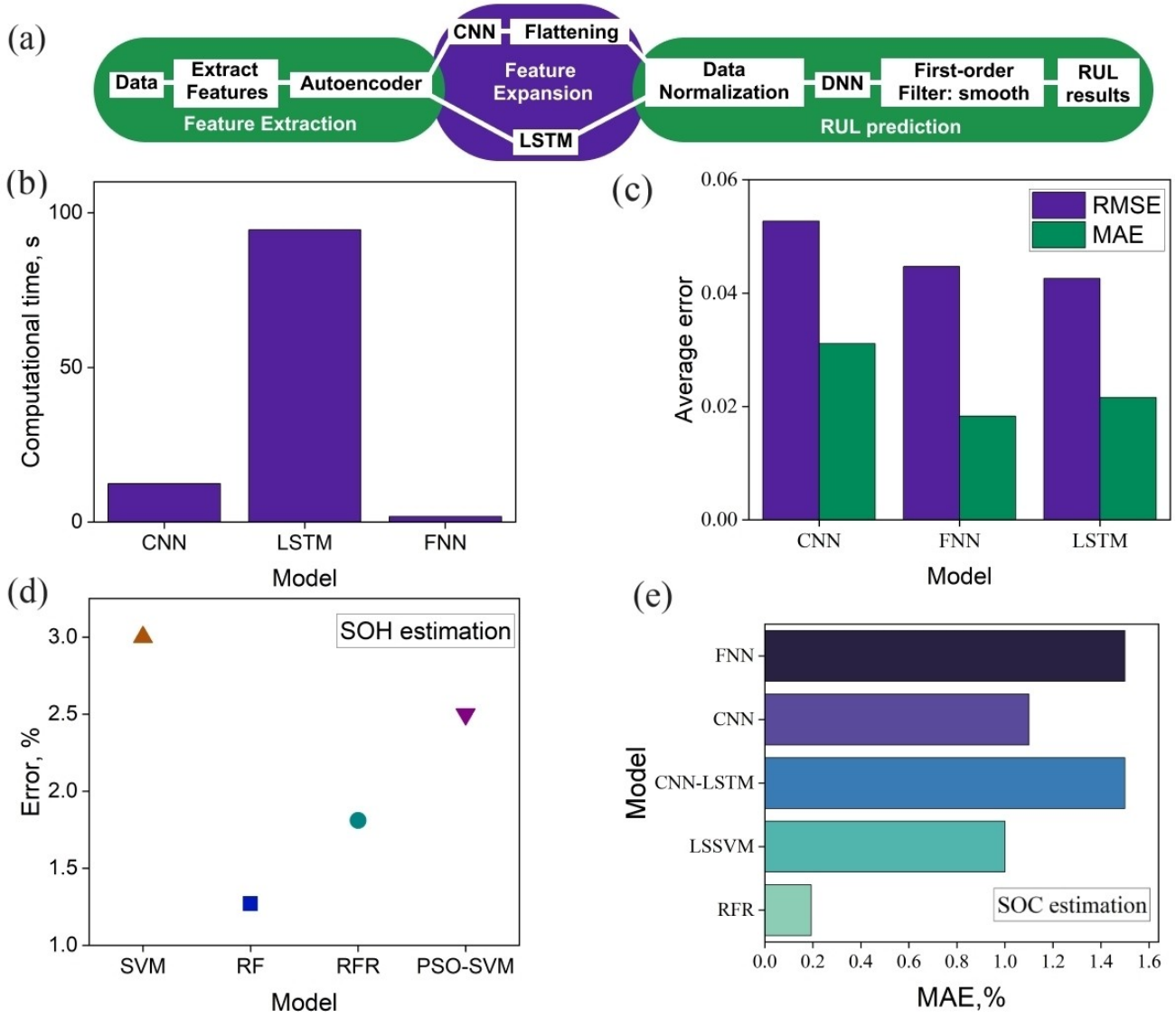

Figure 10. (a) A Novel CNN-LSTM framework for predicting LIB RUL.[112] (b) Average training computational time and (c) RMSE, MAE from the test performance of FNN, CNN, and LSTM.[118] (d) RFR,[155] LSSVM,[125] CNN-LSTM,[114] CNN,[103] FNN[99] models and their MAE in SOC estimation. (e) Average SOH error in different AI models: SVM,[122] PSO-SVM,[134] RF,[152] and RFR.[154]

Another excellent non-interpretable AI method, in addition to neural networks, is support vector machines (SVMs). SVMs excel in the battery production industry for addressing quality classification problems because they can find classes that are hyperplane-separated with a maximum margin.[121] Additionally, SVMs are advantageous for small-sized battery production datasets, as larger training datasets increase the number of support vectors, thereby raising the computational load. Choosing the appropriate kernel function is crucial, as it significantly impacts SVM effectiveness. Common applications of SVMs include online estimation of SOH,[122,123] SOC,[124–128] RUL,[129–131] and fault detection[132] are common applications of this method. Beyond this, SVMS can review sensor data, identify differences and their causes, and ensure that the appropriate steps are taken to ensure that machines are operational at all times.

Feng et al.[122] trained, verified, and evaluated SVM models for online SOH calculation in commercial LIBs with NCM cathode, having an error of less than 3% in 95% of cases. A significant performance enhancement for classification with regression was achieved, and RUL was calculated using a multistage technique.[129] This two-step procedure involved gross RUL estimation through classification and precise RUL estimation via regression analysis. With 196 discharge cycles, the average computation time was 1.26 ms for multiple battery data, and the regression model test data RMSE was 0.2420%. For single battery data, the classification model showed 96.61% accuracy, correctly classifying 57 out of 59 cycles, while the regression model had an RMSE of 0.16554%.

An SVM variation known as least squares support vector machines (LSSVM) trains using least squares principles instead of quadratic programming. LSSVMs are especially useful for

both classification and regression applications. Li et al. overcame the model's reliance on internal battery variables by utilizing the sliding window method-based LSSVM.[125] They proposed a new LSSVM model with numerous feedback vectors to enhance SOC accuracy. The experimental outcomes demonstrated the excellent accuracy and resilience of the proposed model, with SOC estimation errors reduced to within 1% at higher temperatures.

When combined with SVMs, particle swarm optimization (PSO) may enhance the model global search capability and computation performance.[124,131,133–139] The PSO-SVM model has been demonstrated as the best option for estimating SOH of LFP and NCA cathodes, with an RMSE lower than 2.5%, outperforming other models.[134] This model mitigates the overfitting issue and enhances generalization capacity by using k-fold cross-validation. A novel strategy to increase SOC estimation precision involves incorporating data-driven modeling with an unscented Kalman filter and LSSVM-PSO.[140] This method significantly improves upon previous approaches, maintaining maximum SOC error under different operating conditions at 0.5%.

Tree-based machine learning algorithms, including decision trees (DTs), random forests (RFs), and other specific models, have become highly successful tools for forecasting characteristics and enhancing LIB performance. These models contribute significantly to LIB development and research by providing accuracy, durability, and scalability. Employing a flowchart architecture and accurately mapping non-linear relationships, tree-based approaches offer strong interpretability, making the linkages relevant to battery manufacturing clear. DTs are straightforward yet effective models that recursively divide data according to attributes to generate predictions.[141–146] In DTs, each internal node represents a feature, each branch represents a choice made based on that feature, and each leaf node represents the final conclusion. However, the structure of DTs is easily modified, which can make them unstable and unsuitable for modeling highly nonlinear battery behaviors.[121] A particularly successful example is the RUBoost-based ensemble learning framework, proposed to identify LFP and LTO electrodes based on their half-cell capacity, thickness, and electronic conductivity.[147] In this framework, DTs are used as the weak learners, and adding more DTs can improve classification accuracy. The RUBoost-based model includes three primary hyperparameters: the number of decision trees (M), the learning rate (r), and the desired percentage (P%) of total samples represented by the minority class. As more DTs are applied, the classification error of conductivity tests decreases progressively, converging to 0.13 after 90 DTs for LFP and to 0.14 after 76 DTs for LTO electrodes (Figure 8b). Remarkable classification results were achieved for electrode capacities, with 94.4% accuracy for LTO and 97.8% for LFP. Notably, only three DTs were used to estimate LFP capacity with an error of 0.02%, suggesting a roughly linear relationship between these formulation factors and electrode capacity.

Random forest (RF) is a powerful machine learning algorithm that leverages the outputs of several decision trees (DTs) to handle both classification and regression tasks effectively (Figure 7b).[148–154] RF offers significant advantages over individual DTs, primarily due to its ability to manage complex datasets with intricate feature relationships and its resistance to overfitting. This technique has been widely utilized in numerous fields related to LIB manufacturing, including of online capacity,[149] SOC,[155] and SOH[152,153] estimations. Moreover, RF serves as an excellent alternative to the commonly used equivalent circuit model (ECM) in battery management systems (BMS) due to its precision and reliability. Leveraging trained random forest regressors, ML analysis of the low rate charge curves produced by the mechanistic model has been carried out for LFP, NMC, and NCA cells with an RMSE of 5%.[156] Li et al.[149] presented a low computational cost RF regression (RFR) method to estimate the battery capacity of NMC cells under various aging scenarios, achieving an RMSE of less than 1.3%. The input data for training and testing the framework was the charging capacity data acquired at precise intervals within a specific voltage band. RF demonstrated superior performance compared to incremental capacity (IC) analysis in every test concerning RMSE. Additionally, RFR required no preselection of parameters and proved highly resistant to predictor noise.

In tree-based algorithms, ensemble techniques like bagging[157] and boosting[158] may be employed to combine several different individual models to increase prediction performance.[159–164] Bagging reduces the variance of predictions by combining the output of several classifiers based on various subsamples of the same dataset. A comparative framework was established to examine the effectiveness of bagging and boosting when trained using two distinct predictor vectors.[161] The training technique was illustrated graphically (Figure 8a) to emphasize the primary distinctions between the two methods. The normalized root mean square error (NRMSE) was calculated as follows:

$$NRMSE = \frac{1}{Q_0}\sqrt{\frac{\sum_{i=1}^{N}\left(Q_i-\hat{Q}_i\right)^2}{N}} \tag{14}$$

where Q_0 is the capacity at the beginning of life. With a testing error of about 4%, it was discovered that the bagging methodology outperformed the boosting method in general. The key control parameters, such as mass loading, capacity, and thickness, were measured with a small error using gradient-boosted trees, yielding a very useful result for LIB manufacture.[165]

Another interpretable AI algorithm, linear regression,[166–170] provides a straightforward framework for comprehending the complex correlations between different manufacturing variables and LIB performance. By systematically analyzing data gathered from various manufacturing phases (electrode composition, cell characteristics, and testing outcomes), linear regression can offer valuable insights. For instance, generalized linear models (GLM) and multiple linear regression (MLR) have been utilized to forecast the state of charge (SOC) of cylindrical batteries.[170] Among these, MLR combined with particle swarm optimization (MLR-PSO) emerged as the most successful predictor in every case study, yielding the best overall results for both training and test sets. The training of linear regression models is

computationally efficient, producing results that are straightforward to understand and capable of handling inaccurate data well. However, in practical applications, linear relationships may not always be accurate, and linear regression might perform poorly when dealing with complex issues. For example, when nonlinear interactions between variables are significant, the limitations of linear regression become apparent, making it less suitable for such scenarios compared to more advanced algorithms.

3.2.2.1. Post-Manufacturing Quality Assurance

Post-manufacturing quality assurance is crucial for preventing battery failures before they reach customers. Due to their high accuracy and elimination of human error, digital decisions such as those made by AI are attractive options for manufacturers. Neural networks, particularly deep learning models, can accurately measure multidimensional test data (Figures 10d,e) and identify minor errors during battery tests.

AI algorithms, including CNN, ADNN, SVM, and RF, are able to forecast a battery's RUL[92,112,115–117,129–131,137,150] and suggest preventative actions to avoid failures, which is especially critical in scenarios where battery failure could have serious consequences. These AI models can continuously monitor the production process and recognize deviations from the norm that may indicate defects. Integrating AI algorithms for real-time control with continuous monitoring ensures timely detection of quality issues during production.[95,122,123,128,134,149,155] Furthermore, monitoring the state of charge (SOC) and state of health (SOH) is essential for tracking battery performance and longevity. AI-based modeling approaches can enhance these monitoring capabilities, providing accurate and real-time data.[94,97–99,103–106,122–128,152–153,155] AI-based degradation analysis significantly improves post-manufacturing quality assurance of LIBs. Advanced AI models such as CNNs,[110] SVMs, RFs,[156] and LSTM networks analyze large datasets to detect and predict decay trends with high accuracy.

The implementation of AI-based quality control systems enhances the production of high-energy density batteries by recognizing defects, estimating deterioration and aging rates, and ultimately extending battery lifespan. By employing these state-of-the-art methods, manufacturers can improve quality assurance systems and deliver more efficient and superior next-generation batteries to the market.

3.2.3. Modeling the Energy Consumption and Cost for Battery Manufacturing

To make manufacturing efficient, sustainable, and low-cost, it is crucial to understand the most energy-consuming processes and materials involved (Figure 11). Modeling plays a significant role in determining and reducing the carbon footprint associated with battery manufacturing.[171–177] For instance, the drying process consumes the majority of energy during electrode production.[178–180,37] Consequently, manufacturers need to reconsider their strategy for solvent selection, especially regarding the hazardous N-methyl-2-pyrrolidone (NMP), which has a high boiling point of 204 °C. Reducing the solvent amount by 60% can lead to faster drying and coating rates, resulting in a 9% decrease in total energy cost.[181] To assist industries in

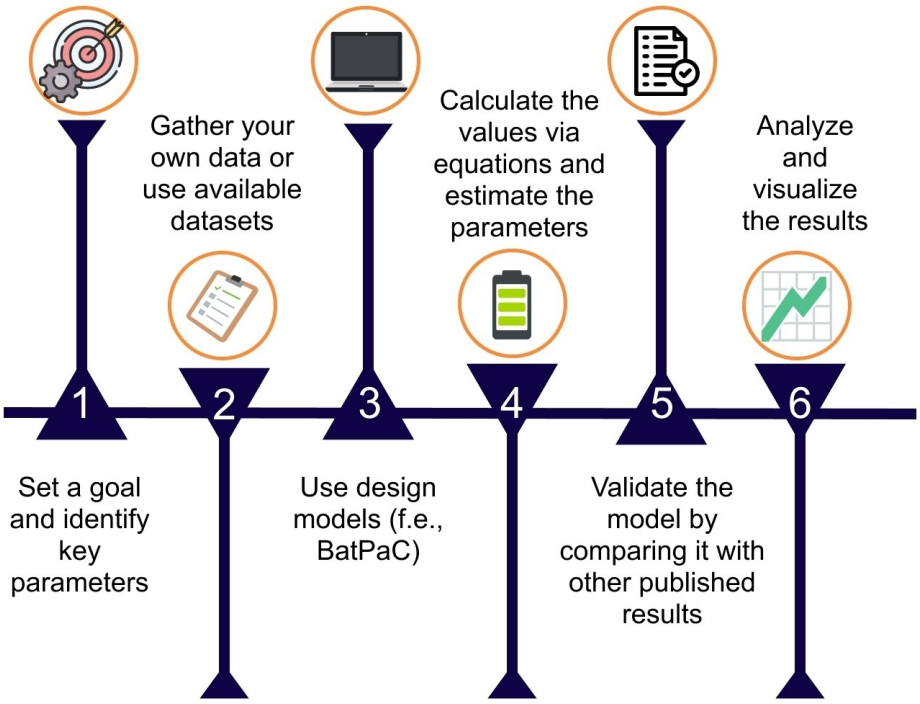

Figure 11. A step-by-step roadmap of cost and energy consumption modeling of batteries, including 6 steps from setting goals to visualizing results.

developing more sustainable practices, modern analytical tools like life cycle assessment (LCA)[182–184] and data-driven modeling approaches should be implemented throughout the entire process, from raw material extraction to the assembly of cells and packs. These tools help identify critical areas for improvement, optimize resource use, and minimize environmental impact. By integrating these methodologies, manufacturers can achieve greater efficiency and sustainability in battery production while reducing costs.

A calculation model of energy consumption based on the heat balance was proposed, determining the evaporation rate of NMP in NMC cathodes.[178] It was found that the average energy consumption of electric heating increases by 56.70 kW with each 1 m/s rise in inlet wind speed. Ahmed et al.[37] calculated the energy consumption and expenses associated with drying and recovering NMP using a spreadsheet approach. Their findings showed that a 10 kWh battery pack requires 421 kWh of energy for production. This high energy demand is primarily due to the substantial volume of air that must be heated and cooled, which varies with the time of year and location. For example, a 5% increase in total energy is needed when the ambient air temperature rises from 0 to 40 °C.

In 2023, a comprehensive complex model and framework were developed (Figure 12a)[171] to enhance battery design and manufacturing. This model included 20,736 different material choices covering their pricing, carbon emissions, material criticality, and energy density. Based on the BatPac battery design model, the following strategies were identified as the most effective: (1) Minimal Criticality: Synthetic graphite anodes and LFP cathodes; (2) Minimized Carbon Footprint: Synthetic graphite anodes and LMO cathodes; (3) Cost Reduction: Natural graphite anodes and LMO cathodes; and (4) Optimal Energy Density: Natural graphite anodes and NMC811 cathodes. Additionally, two major strategies were created, *i.e.*, combining various cathode active materials and reducing the weight of structural parts at the battery and vehicle levels.

The interaction between battery design and cost for transportation applications is represented by the Battery Performance and Cost (BatPaC) model.[185–188] This model specifically analyzes trade-offs resulting from varying user needs and predicts the cost of producing lithium-ion batteries (LIBs). By providing comprehensive cost breakdowns and performance characteristics based on actual data and advanced modeling methodologies, BatPaC is a valuable tool for battery development. For example, Wang et al.[189] used the BatPac model to approximate the cost of a LIB pack using silicon nanowires (SiNW) as the anode and NMC111 as the cathode. They discovered that switching the anode material from graphite to SiNW reduced the battery weight by 83 kg, the specific energy cost by $9/kWh, and the overall battery cost by $570.

The global warming potential (GWP), which measures the total greenhouse gas emissions related to batteries, is typically represented in kg CO_2 and is the most frequently studied environmental effect in energy systems.[190–193] For example, recycled LFP batteries have a greater GWP than NMC.[194] Among recycling processes, the combined hydro-pyrometallurgical process performs best in terms of energy usage, whereas pyrometallurgy is the least efficient.

Recycling lithium-ion batteries (LIBs) is recommended over landfilling as it reduces energy consumption, minimizes greenhouse gas emissions, and conserves significant natural resources.[195,196] A dynamic simulation model based on system dynamics principles was used to examine energy consumption and GHG emissions during the recycling process. Energy consumption was measured using the following equation:

$$E_f(t) = M_f(t) \times \sum_1^n \sigma_n \quad (15)$$

where $E_f(t)$ is the flow of energy consumption in different processes and $M_f(t)$ is the amount of material in the flow in the year t, σ_n is the energy required per one tonne of LCE. The findings demonstrated that recycling LIBs helps prevent shortages of essential minerals from a mass flow perspective.

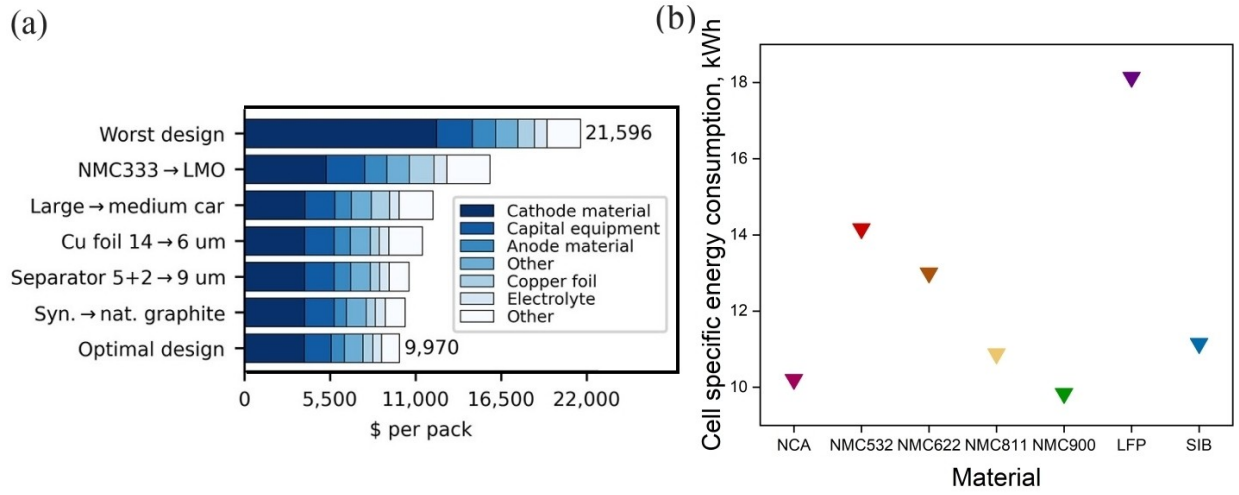

Figure 12. (a) Pack-level battery cost in US dollars for 500,000 packs produced annually in Europe at a factory scale.[171] (b) Calculated energy consumption (kWh_{prod}) for the manufacturing of LIB and PLIB cells was per kWhcell of cell energy generated.[197]

However, from an environmental standpoint, recovering lithium from LIBs using current technology is not recommended as it results in 38–45% greater energy consumption and 16–20% more air emissions than its initial manufacture.

For cost modeling, the BatPaC model was utilized to design 90 Wh cells with various cathode materials (LFP, NMC111, NCA, and LMO), estimating the cost for an annual production of 10 million cells.[198] The production costs, including those for electrodes, cell stacking, cell filling, and formation expenses, were separated from other process costs, such as overhead and fees. It was recommended to double the electrode's thickness to reduce battery costs by 25%. Due to their low energy density per kilogram and cubic centimeter, LFP and LMO cells were the most expensive in terms of energy cost per kWh. The cost of prismatic pouch cell designs using synthesized Li_{1+x} $(Mn_{4/9}Co_{1/9}Ni_{4/9})_{1-x}O_2$ with two lithium content levels (x = 0 and 0.05) was also evaluated via the BatPaC model.[199] A battery pack with the $Li_{1.05}$ $(Mn_{4/9}Co_{1/9}Ni_{4/9})_{0.95}O_2$ cathode was predicted to have the best energy density and lowest cost. Because of its high mass energy density and greater stability at higher voltages, less material was used, which resulted in a smaller cell and a lower cost.

Several research studies have examined the bottom-up cost model, accounting for various specific parts and production techniques.[200,201] It was reported that a modular theoretical bottom-up battery Cell Energy and Cost model (CellEst) was created.[200] CellEst design enables an examination of how changes in raw material prices affect the overall cost of battery packs. The first manufacturing model comparing the costs of prismatic and cylindrical cells was reported by Ciez in 2017.[202] They implemented a process-based cost model (PBCM) to calculate the costs of different chemistries (LMO, NMC, or NCA), cell height and diameter, and electrode thickness. It was found that the cost per kWh for larger prismatic cells was lower for all three battery chemistries compared to cylindrical cells. Additionally, a 200% rise in lithium carbonate pricing resulted in a 10% increase in cost per kWh.

Understanding and optimizing the affordability, technological development, and ecological impact of batteries require effective cost modeling (Table 3). According to the data gathered and published (Figure 13), the NaNMC cathode had the best correlation between cost and energy, while the more widespread Li-ion NMC cathode demonstrated the best energy cost despite the high price of raw materials. Furthermore, reducing the thickness of the electrodes could lower manufacturing costs.

4. Concluding Remarks

The model-driven manufacturing of high-energy-density batteries has demonstrated immense potential in advancing the efficiency, reliability, and cost-effectiveness of battery production. This review has underscored the significant impact of integrating computational models and simulations with experimental manufacturing processes. These advancements have been instrumental in optimizing performance and ensuring stringent quality assurance standards in battery manufacturing. By leveraging advanced modeling techniques, including electrochemical, thermal, and mechanical models, along with AI and ML-driven simulations, researchers have been able to elucidate the intricate interplay of materials, design, and manufacturing parameters.

4.1. Challenges

Despite these advancements, several challenges need to be addressed to fully realize the potential of model-driven manufacturing:

(1) Model validation and parameter sensitivity.

One of the primary challenges is ensuring the accuracy and robustness of models across different scales and conditions. Validating these models in real-world applications remains complex, as small deviations in model parameters can lead to significant discrepancies in predictions. It is crucial to develop standardized validation protocols and improve the sensitivity analysis of these models to enhance their reliability.

Table 3. Cost analysis of LIBs and SIBs based on BatPaC modeling.

Materials	Technology	Year	Thickness of cathode, μ	Type of cell	Cost, $/kWh
NMC-Gr[198]	Li-ion	2015	100	pouch	233
NMC-Gr[202]	Li-ion	2017	100	cylindrical	180
NMC-Gr[189]	Li-ion	2020	80	pouch	169
NMC-Gr[203]	Li-ion	2015	100	prismatic	188
NMC/SiNWs[189]	Li-ion	2020	76	pouch	160
NCA/Gr[198]	Li-ion	2015	100	pouch	243
NCA/Gr[202]	Li-ion	2017	100	cylindrical	206
LMO/Gr[198]	Li-ion	2015	100	pouch	263
LMO/Gr[203]	Li-ion	2015	100	prismatic	226
LFP/Gr[198]	Li-ion	2015	100	pouch	285
NaNMC/HC[187]	Na-ion	2022	237	prismatic	124
NMMT/HC[204]	Na-ion	2019	82	cylindrical	241

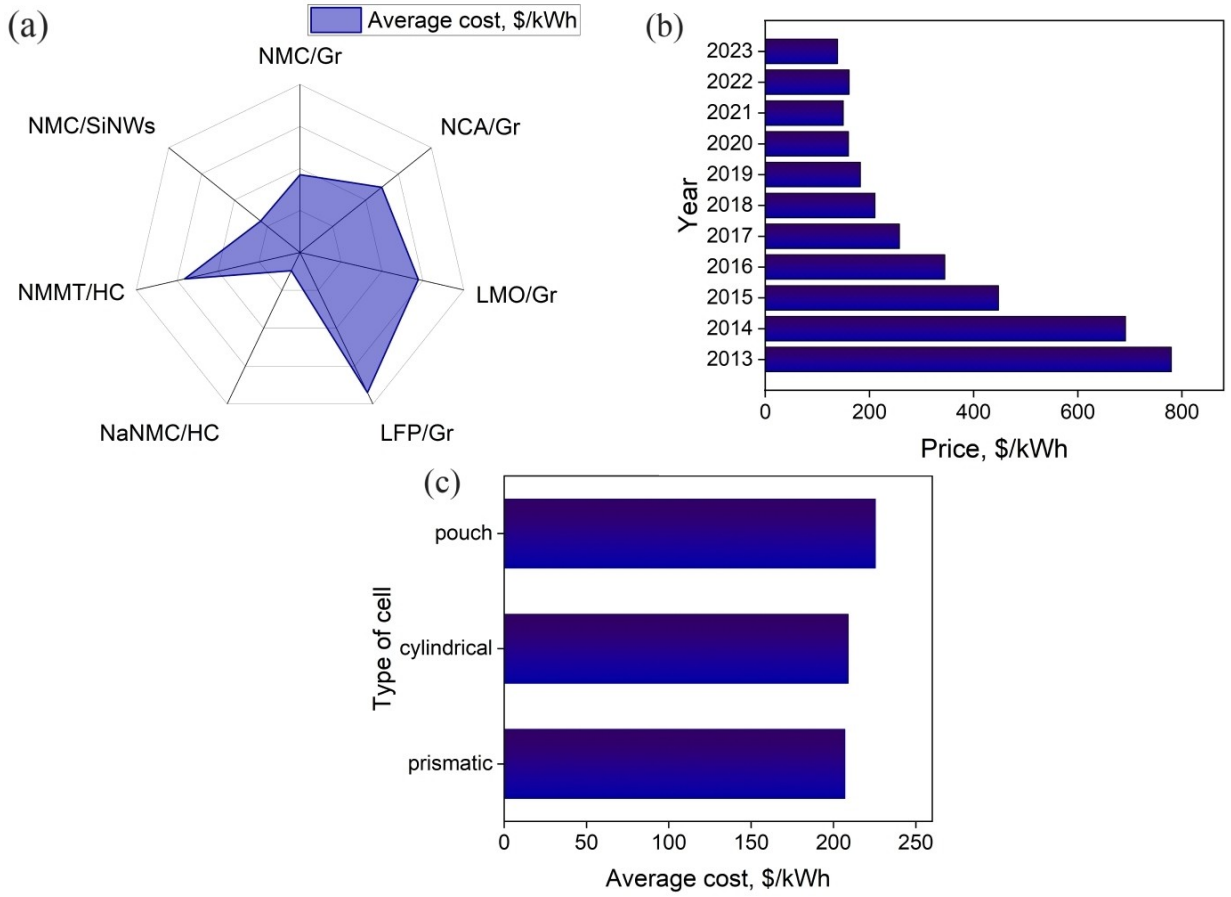

Figure 13. Correlation between average cost in $/kWh and type of (a) materials for LIBs and SIBs and (c) cells for LIBs. (b) LIB pack price worldwide from 2013 to 2023 based on Statista.[205]

(2) Integration of AI and machine learning.

While the integration of AI and machine learning into predictive modeling and process optimization holds great promise, it is still in its early stages. The development of more sophisticated algorithms that can handle the complexities of battery manufacturing processes is essential. Additionally, ensuring the interpretability and transparency of AI-driven models is crucial for their widespread adoption in the industry.

(3) Scaling Up.

Transitioning from laboratory-scale demonstrations to industrial-scale applications poses numerous challenges. High-throughput data acquisition and real-time processing capabilities are required to handle the vast amounts of data generated during manufacturing. Developing scalable algorithms that can efficiently process this data and provide actionable insights is critical for successful implementation.

(4) Energy Consumption and Environmental Impact.

Battery manufacturing is an energy-intensive process, and reducing energy consumption while minimizing environmental impact is a significant challenge. Innovative solutions, such as optimizing solvent selection and implementing energy-efficient drying techniques, are necessary to address this issue. Additionally, incorporating life cycle assessment (LCA) and data-driven approaches can help identify areas for improvement and enhance the sustainability of battery production.

4.2. Future Opportunities

The future of model-driven manufacturing for high-energy-density batteries is promising, with numerous opportunities for further advancements:

(1) Development of Advanced AI and ML Algorithms.

Ongoing research and development of more sophisticated AI and ML algorithms will enhance the accuracy and efficiency of predictive models. These advancements will enable better process optimization and quality control, leading to improved battery performance and reliability. In the meantime, security and resilience of AI-driven manufacturing are essential elements in model-driven manufacturing.

(2) Interdisciplinary collaboration.

Collaboration between material scientists, engineers, and data scientists will be crucial in driving innovation and overcoming current limitations. Interdisciplinary research initiatives can foster the development of new materials, processes, and technologies that can be integrated into model-driven manufacturing approaches.

(3) Sustainable manufacturing practices.

Adopting sustainable manufacturing practices is essential for reducing the environmental impact of battery production. Integrating LCA and data-driven approaches can help identify critical areas for improvement, optimize resource use, and minimize waste. Additionally, exploring alternative materials and processes that have lower environmental footprints can further enhance sustainability.

(4) Real-Time monitoring and control.

Implementing real-time monitoring and control systems will enable manufacturers to detect deviations and anomalies during the production process promptly. This capability can significantly improve quality assurance and reduce the likelihood of defects, leading to more reliable and consistent battery performance.

(5) Advanced materials and design:

The development of new materials with enhanced properties, such as higher energy density and improved stability, will continue to drive advancements in battery technology. Model-driven approaches can facilitate the design and optimization of these materials, ensuring that they meet the specific requirements of various applications.

(6) Regulatory and Standardization Efforts:

Establishing industry-wide standards and regulations for model-driven manufacturing practices can help ensure consistency and reliability across the sector. Regulatory frameworks that promote the adoption of advanced modeling techniques and sustainable practices will be instrumental in driving the widespread implementation of these approaches.

In summary, the model-driven manufacturing of high-energy-density batteries represents a transformative approach with the potential to revolutionize the industry. By addressing current challenges and leveraging future opportunities, this approach can lead to the development of more efficient, reliable, and sustainable battery technologies. Continued research, innovation, and collaboration will be essential in meeting the growing demands for energy storage solutions and ensuring a sustainable future for battery manufacturing.

Author Contributions

Daria Maksimovna Vakhrusheva: Methodology, data analysis, and writing – original draft. **Jun Xu**: Conceptualization, supervision, and writing – review & editing.

Acknowledgements

JX was supported by the Startup Funding from the University of Delaware.

Conflict of Interests

The authors declare that they have no known competing financial interests or personal relationships that could have appeared to influence the work reported in this paper.

Keywords: Battery manufacturing · Model-driven manufacturing · High energy density, · Process optimization · Quality assurance

[1] A. Yoshino, *Angew. Chem. Intern. Ed.* **2012**, *51*(24), 5798–5800.
[2] M. Abdelbaky, et al., *Cleaner Logistics and Supply Chain* **2023**, *9*, 100130.
[3] Y. Liu, et al., *IScience* **2021**, *24*(4), 102332.
[4] L. Zhao, et al., *Adv. Mater.* **2022**, *34*(18), 2106704.
[5] S. Glazier, et al., *J. Electrochem. Soc.* **2017**, *164*(14), A3545.
[6] C. Wang, A. J. Appleby, F. E. Little, *J. Electroanal. Chem.* **2001**, *497*(1), 33–46.
[7] M. Yoshio, H. Wang, K. Fukuda, *Angew. Chem. Intern. Ed.* **2003**, *42*(35), 4203–4206.
[8] M. Ratynski, et al., *Carbon* **2019**, *145*, 82–89.
[9] L. Xie, et al., *Adv. Energy Mater.* **2021**, *11*(38), 2101650.
[10] Y. Shen, et al., *Small* **2020**, *16*(7), 1907602.
[11] E. Buiel, J. R. Dahn, *Electrochim. Acta* **1999**, *45*(1), 121–130.
[12] H. Wang, et al., *Electrochem. Energy Rev.* **2019**, *2*(4), 509–517.
[13] Y. Zhang, et al., *Mater. Today* **2020**, *33*, 56–74.
[14] J. Lang, et al., *Energy Storage Mater.* **2017**, *7*, 115–129.
[15] S. Li, et al., *Energy Storage Mater.* **2020**, *32*, 306–319.
[16] H. Zhang, et al., *Angew. Chem. Intern. Ed.* **2018**, *57*(46), 15002–15027.
[17] Y. Ma, et al., *Energy Storage Mater.* **2018**, *11*, 197–204.
[18] G. Wang, et al., *Energy Storage Mater.* **2019**, *23*, 701–706.
[19] T. Chen, et al., *J. Power Sources* **2017**, *363*, 126–144.
[20] K. Schulmeister, W. Mader, *J. Non-Cryst. Solids* **2003**, *320*(1), 143–150.
[21] A. Hirata, et al., *Nat. Commun.* **2016**, *7*(1), 11591.
[22] A. R. Kamali, D. J. Fray, *Rev. Adv. Mater. Sci.* **2011**, *27*(1), 14–24.
[23] Z. Hu, et al., *Coord. Chem. Rev.* **2016**, *326*, 34–85.
[24] H. Zhang, et al., *InfoMat* **2022**, *4*(4), e12228.
[25] Y.-B. He, et al., *J. Power Sources* **2013**, *239*, 269–276.
[26] P. He, et al., *J. Mater. Chem.* **2012**, *22*(9), 3680–3695.
[27] W. Li, S. Lee, A. Manthiram, *Adv. Mater.* **2020**, *32*(33), 2002718.
[28] B. E. Murdock, K. E. Toghill, N. Tapia-Ruiz, *Adv. Energy Mater.* **2021**, *11*(39), 2102028.
[29] G. Liang, et al., *J. Mater.Chem. A* **2020**, *8*(31), 15373–15398.
[30] A. Eftekhari, *J. Power Sources* **2017**, *343*, 395–411.
[31] R. Gupta, et al., *J. Mater. Sci.: Mater. Electron.* **2017**, *28*(7), 5192–5199.
[32] C. Padwal, et al., *Advanced Energy and Sustainability Research* **2022**, *3*(1), 2100133.
[33] Y. Chen, et al., *J. Mol. Liq.* **2023**, *391*, 123410.
[34] S. Mallakpour, M. Dinari, *Green Solvents II: Properties and Applications of Ionic Liquids* (Eds: A. Mohammad, D. Inamuddin), Springer Netherlands, Dordrecht **2012**, 1–32.
[35] J. Li, et al., *Iscience* **2020**, *23*(5), 101081.
[36] D. L. Wood, et al., *Dry. Technol.* **2018**, *36*(2), 234–244.
[37] S. Ahmed, et al., *J. Power Sources* **2016**, *322*, 169–178.
[38] M. Wang, et al., *J. Electrochem. Soc.* **2023**, *170*(1), 010541.
[39] X. Zhang, et al., *Extreme Mech. Lett.* **2015**, *4*, 61–75.
[40] B. Lu, et al., *Phys. Chem. Chem. Phys.* **2016**, *18*(6), 4721–4727.
[41] S. Han, Y. Tang, S. Khaleghi Rahimian, *J. Power Sources* **2021**, *490*, 229571.
[42] V. Laue, F. Röder, U. Krewer, *J. Appl. Electrochem.* **2021**, *51*(9), 1253–1265.
[43] A. Tulsyan, et al., *J. Power Sources* **2016**, *331*, 208–223.
[44] A. Zülke, et al., *J. Electrochem. Soc.* **2021**, *168*(12), 120522.
[45] M. Guo, G. Sikha, R. E. White, *J. Electrochem. Soc.* **2010**, *158*(2), A122.
[46] J. Tian, Y. Wang, Z. Chen, *J. Clean. Prod.* **2021**, *278*, 123456.
[47] T. F. Fuller, M. Doyle, J. Newman, *J. Electrochem. Soc.* **1994**, *141*(1), 1.
[48] M. Guo, G.-H. Kim, R. E. White, *J. Power Sources* **2013**, *240*, 80–94.
[49] K.-Y. Oh, et al., *J. Power Sources* **2016**, *326*, 447–458.
[50] C. Blanc, A. Rufer, *Multiphysics and Energetic Modeling of a Vanadium Redox Flow Battery*, IEEE International Conference on Sustainable Energy Technologies, Singapore, **2008**, 696–701.

[51] C. Liu, L. Liu, *J. Electrochem. Soc.* **2017**, *164*(11), E3254.
[52] M. T. Castro, et al., *J. Energy Storage* **2021**, *42*, 102982.
[53] A. A. Franco, *RSC Adv.* **2013**, *3*(32), 13027–13058.
[54] C. Zhang, et al., *J. Power Sources* **2015**, *290*, 102–113.
[55] J. Smekens, et al., *Electrochim. Acta* **2015**, *174*, 615–624.
[56] S. Yin, et al., *J. Power Sources* **2020**, *476*, 228532.
[57] P. P. Kumar, et al., *Phys. Chem. Chem. Phys.* **2023**, *25*(30), 20462–20472.
[58] M. Wang, X. Xiao, X. Huang, *J. Power Sources* **2017**, *348*, 66–79.
[59] A. Ghahremani, A. E. Fathy, *Energy Sci. Eng.* **2015**, *3*(6), 520–534.
[60] B. Liu, et al., *J. Power Sources* **2020**, *450*, 227667.
[61] Y. Chen, et al., *J. Power Sources* **2022**, *527*, 231178.
[62] S. Ansah, et al., *Comput. Mater. Sci.* **2021**, *196*, 110559.
[63] Q. Hu, et al., *Solid State Ion.* **2024**, *406*, 116471.
[64] D. Shi, et al., *J. Power Sources* **2011**, *196*(19), 8129–8139.
[65] X. Xiao, W. Wu, X. Huang, *J. Power Sources* **2010**, *195*(22), 7649–7660.
[66] W. Wu, et al., *Comput. Mater. Sci.* **2014**, *83*, 127–136.
[67] N. Lin, F. Röder, U. Krewer, *Energies* **2018**, *11*(11), 2998.
[68] K. Kuchler, et al., *Model. Simul. Mater. Sci. Eng.* **2018**, *26*(3), 035005.
[69] J. Feinauer, et al., *Comput. Mater. Sci.* **2015**, *109*, 137–146.
[70] B. Prifling, et al., *Comput. Mater. Sci.* **2021**, *192*, 110354.
[71] C. Liu, *Revealing Lithium-Ion Battery Internal Uncertainty through a Combined Electrochemical Based Degradation Battery Model with a Markov Chain Monte Carlo Approach*, SAE Technical Paper 2020-01-0450, **2020**.
[72] J. Guo, Z. Li, M. Pecht, *J. Power Sources* **2015**, *281*, 173–184.
[73] A. Chu, et al., *J. Power Sources* **2020**, *478*, 228991.
[74] C. Yang, et al., *IEEE Transact. Ind. Electron.* **2019**, *67*(11), 9659–9670.
[75] E. Ayerbe, et al., *Adv. Energy Mater.* **2022**, *12*(17), 2102696.
[76] L. Zhang, et al., *J. Power Sources* **2022**, *541*, 231568.
[77] L.Liu, et al., *Kinetic Monte Carlo simulation of lithium dendrite growth in lithium-ion battery*, 2021 IEEE 4th International Electrical and Energy Conference (CIEEC), Wuhan, China, **2021**, 1–5.
[78] E. M. Gavilán-Arriazu, et al., *Electrochim. Acta* **2020**, *331*, 135439.
[79] R. N. Methekar, et al., *J. Electrochem. Soc.* **2011**, *158*(4), A363.
[80] E. M. Gavilán-Arriazu, et al., *J. Electrochem. Soc.* **2019**, *167*(1), 01353383, DOI: 10.1149/1945-7111/ab798a.
[81] O. Schmidt, et al., *J. Electrochem. Soc.* **2020**, *167*(6), 060501.
[82] W. Van Gunsteren, H. Berendsen, *Mol. Phys.* **1982**, *45*(3), 637–647.
[83] M. Zhu, J. Park, A. Sastry, *J. Electrochem. Soc.* **2011**, *158*(10), A1155.
[84] M. Cerbelaud, et al., *Langmuir* **2012**, *28*(29), 10713–10724.
[85] P. J. Bond, et al., *J. Struct. Biol.* **2007**, *157*(3), 593–605.
[86] S. S. Cho, D. L. Pincus, D. Thirumalai, *Proc. Nat. Acad. Sci.* **2009**, *106*(41), 17349–17354.
[87] J. Li, et al., *J. Electroanal. Chem.* **2022**, *917*, 116380.
[88] X. Yao, et al., *J. Mater. Proc. Technol.* **2023**, *321*, 118154.
[89] Y. Wang, et al., *Appl. Therm. Eng.* **2023**, *228*, 120482.
[90] M.-F. Ng, et al., *Nat. Mach. Intel.* **2020**, *2*(3), 161–170.
[91] T. Zahid, et al., *Energy* **2018**, *162*, 871–882.
[92] A. Nuhic, et al., *J. Power Sources* **2013**, *239*, 680–688.
[93] B. Wu, et al., *J. Power Sources* **2018**, *395*, 128–136.
[94] M. Charkhgard, M. Farrokhi, *IEEE Transact. Ind. Electron.* **2010**, *57*(12), 4178–4187.
[95] M. Naguib, et al., *Accurate Surface Temperature Estimation of Lithium-Ion Batteries Using Feedforward and Recurrent Artificial Neural Networks*, 2021 IEEE Transportation Electrification Conference & Expo (ITEC), Chicago, IL, USA, **2021**, 52–57.
[96] G. Dziechciaruk, et al., *J. Energy Storage* **2020**, *31*, 101503.
[97] B. P. Adedeji, G. Kabir, *Decis. Anal. J.* **2023**, *8*, 100255.
[98] C. Vidal, et al., *SAE Intern. J. Adv. Curr. Prac. Mobil.* **2020**, *2*(*2020-01-1181*), 2872–2880.
[99] V. Indragandhi, S. Vedhanayaki, *Robust feedforward neural network-based state of charge estimation of lithium-ion batteries*, AIP Conference Proceedings, AIP Publishing, **2024**, 2966 (1): 040018.
[100] L. Xie, A. Yuille, *Genetic CNN*, 2017 IEEE International Conference on Computer Vision (ICCV), Venice, Italy, **2017**, 1388–1397.
[101] J. Wu, *National Key Lab for Novel Software Technology*, Nanjing University, China, **2017**, 5(*23*), 495.
[102] R. Chauhan, K. K. Ghanshala, R. C. Joshi, *Convolutional Neural Network (CNN) for Image Detection and Recognition*, 2018 First International Conference on Secure Cyber Computing and Communication (ICSCCC), Jalandhar, India, **2018**, 278–282.
[103] X. Fan, et al., *Energy* **2022**, *256*, 124612.
[104] E. Chemali, et al., *Energies* **2022**, *15*, DOI: 10.3390/en15031185.
[105] X. Gu, et al., *Energy* **2023**, *262*, 125501.
[106] G. Lee, D. Kwon, C. Lee, *Mech. Syst. Signal Process.* **2023**, *188*, 110004.
[107] T. K. Pradyumna, et al., *J. Power Electronics* **2022**, *22*(5), 850–858.
[108] S. Shen, et al., *Appl. Energy* **2020**, *260*, 114296.
[109] C. Qian, et al., *Energy* **2021**, *227*, 120333.
[110] N. Costa, et al., *J. Energy Storage* **2022**, *55*, 105558.
[111] Y. Li, et al., *J. Electrochem. Energy Convers. Storage* **2022**, *19*(3), 030901.
[112] L. Ren, et al., *IEEE Transact. Ind. Inform.* **2021**, *17*(5), 3478–3487.
[113] H. Xu, et al., *Energy* **2023**, *276*, 127585.
[114] X. Song, et al., *IEEE Access* **2019**, *7*, 88894–88902.
[115] D. Li, L. Yang, *J. Electrochem. Energy Convers. Storage* **2021**, *18*(4).
[116] L. Ren, et al., *IEEE Access* **2018**, *6*, 50587–50598.
[117] J. Wei, G. Dong, Z. Chen, *IEEE Trans. Ind. Electron.* **2018**, *65*(7), 5634–5643.
[118] K. Kaur, et al., *Intern. J. Energy Res.* **2021**, *45*(2), 3113–3128.
[119] J. Obregon, et al., *J. Energy Storage* **2023**, *60*, 106680.
[120] Y. Choi, et al., *IEEE Access* **2019**, *7*, 75143–75152.
[121] K. Liu, et al., *IEEE/CAA J. Autom. Sin.* **2022**, *9*(7), 1139–1165.
[122] X. Feng, et al., *IEEE Trans. Veh. Technol.* **2019**, *68*(9), 8583–8592.
[123] Z. Chen, et al., *Appl. Sci.* **2018**, *8*(6), 925.
[124] G. Guo, et al., *Adv. Mater. Res.* **2014**, *1051*, 1004–1008.
[125] J. Li, et al., *IEEE Access* **2020**, *8*, 195398–195410.
[126] J. C. Álvarez Antón, et al., *Appl. Math. Model.* **2013**, *37*(9), 6244–6253.
[127] L. Zhang, et al., *IFAC-PapersOnLine* **2019**, *52*(11), 256–261.
[128] L. Zhang, et al., *IEEE Access* **2020**, *8*, 156165–156176.
[129] M. A. Patil, et al., *Appl. Energy* **2015**, *159*, 285–297.
[130] D. Liu, et al., *Measurement* **2015**, *63*, 143–151.
[131] D. Gao, M. Huang, *J. Power Electron.* **2017**, *17*(5), 1288–1297.
[132] S. Chatterjee, et al., *Mater. Today: Proc.* **2023**, *74*, 703–707.
[133] K. Chen, et al., *Green Energy Intell. Transp.* **2024**, *3*(1), 100151.
[134] R. Li, et al., *Front. Energy Res.* **2021**, *9*.
[135] R. Li, W. Li, H. Zhang, *Intern. J. Electrochem. Sci.* **2022**, *17*(2), 220212.
[136] R. Li, et al., *IEEE Access* **2020**, *8*, 10234–10242.
[137] L. Su, *Adv. Eng. Technol. Res.* **2023**, *5*(1), 394–394.
[138] Y. Zhi, H. Wang, L. Wang, *Complex Intel. Sys.* **2022**, *8*(3), 2167–2182.
[139] C. Xu, et al., *IEEE Access* **2021**, *9*, 85232–85239.
[140] Y. Zhou, et al., *Intern. J. Green Energy* **2024**, *21*(2), 376–386.
[141] R. P. Cunha, et al., *Batter. Supercaps* **2020**, *3*(1), 60–67.
[142] A. Turetskyy, et al., *Energy Technol.* **2020**, *8*(2), 1900136.
[143] X. Qiang, et al., *Energy Technol.* **2024**, *12*(3), 2301065.
[144] Z. Zhang, et al., *Intern. J. Energy Res.* **2022**, *46*(2), 1756–1765.
[145] R. Pan, et al., *Energy* **2023**, *285*, 129460.
[146] J. Schnell, et al., *J. Power Sources* **2019**, *413*, 360–366.
[147] K. Liu, et al., *IEEE/ASME Trans. Mech.* **2022**, *27*(5), 2474–2483.
[148] L. Breiman, *Mach. Learn.* **2001**, *45*(1), 5–32.
[149] Y. Li, et al., *Appl. Energy* **2018**, *232*, 197–210.
[150] J. Wu, et al., *Energy Rep.* **2022**, *8*, 313–326.
[151] K. Liu, et al., *IEEE/ASME Trans. Mechatron.* **2021**, *26*(6), 2944–2955.
[152] K. S. R. Mawonou, et al., *J. Power Sources* **2021**, *484*, 229154.
[153] N. Yang, et al., *J. Energy Storage* **2022**, *48*, 103857.
[154] G. Wang, Z. Lyu, X. Li, *Batteries* **2023**, *9*(6), 332.
[155] M. S. H. Lipu, et al., *IEEE Trans. Intel. Veh.* **2023**, *8*(1), 639–648.
[156] K. S. Mayilvahanan, et al., *Batter. Supercaps* **2022**, *5*(1), e202100166.
[157] L. Breiman, *Mach. Learn.* **1996**, *24*(2), 123–140.
[158] R. E. Schapire, *A brief introduction to boosting, in Proceedings of the 16th international joint conference on Artificial intelligence*, Morgan Kaufmann Publishers Inc., Stockholm, Sweden **1999**, *2*, 1401–1406.
[159] P. Bühlmann, *Bagging, Boosting and Ensemble Methods, in Handbook of Computational Statistics: Concepts and Methods* (Eds: J. E. Gentle, W. K. Härdle, Y. Mori), Springer Berlin Heidelberg, Berlin, Heidelberg **2012**, 985–1022.
[160] V. Chandran, et al., *World Electr. Veh. J.* **2021**, *12*(1), 38.
[161] A. Guarino, W. Zamboni, E. Monmasson, *A Comparison of Ensemble Machine Learning Techniques for the Estimate of Residual Capacity of Li-Ion Batteries*, 2020 IEEE 29th International Symposium on Industrial Electronics (ISIE), Delft, Netherlands, **2020**, 1307–1312.
[162] E. Ipek, M. K. Eren, M. Yilmaz, *State-of-Charge Estimation of Li-ion Battery Cell using Support Vector Regression and Gradient Boosting Techniques*, 2019 International Aegean Conference on Electrical Machines and Power Electronics (ACEMP) & 2019 International Conference on Optimization of Electrical and Electronic Equipment (OPTIM), Istanbul, Turkey, **2019**, 604–609.
[163] P. Qin, L. Zhao, Z. Liu, *J. Energy Storage* **2022**, *47*, 103644.
[164] S. Jafari, Z. Shahbazi, Y.-C. Byun, *Energies* **2022**, *15*(13), 4753.
[165] M. F. Niri, et al., *Energy AI* **2022**, *7*, 100129.
[166] D. Maulud, A. M. Abdulazeez, *J. Appl. Sci. Technol. Trends* **2020**, *1*(2), 140–147.

[167] S. Rong, Z. Bao-Wen, The research of regression model in machine learning field, MATEC Web of Conferences, EDP Sciences, **2018**, *176*, 01033.
[168] Y. Khawaja, et al., *Ain Shams Eng. J.* **2023**, *14*(12), 102213.
[169] B. Li, C. M. Jones, V. Tomar, *J. Electrochem. Energy Convers. Storage* **2021**, *18*(4), 040905.
[170] D. Castanho, et al., *Energies* **2022**, *15*(19), 6881.
[171] J. Baars, F. Cerdas, O. Heidrich, *Environ. Sci. Technol.* **2023**, *57*(12), 5056–5067.
[172] L. Lander, et al., *Appl. Energy* **2021**, *289*, 116737.
[173] P. Li, X. Xia, J. Guo, *Sep. Purif. Technol.* **2022**, *296*, 121389.
[174] C. Wang, et al., *J. Clean. Prod.* **2017**, *163*, 241–251.
[175] L. Wang, et al., *J. Clean. Prod.* **2020**, *276*, 124244.
[176] Q. Chen, et al., *J. Clean. Prod.* **2022**, *369*, 133342.
[177] T. Peng, L. Ren, X. Ou, *Energy* **2023**, *282*, 128412.
[178] K. Zhou, et al., *IOP Conf. Ser.: Mater. Sci. Eng.* **2020**, *793*(1), 012057.
[179] C. Yuan, et al., *CIRP Annals* **2017**, *66*(1), 53–56.
[180] M. Thomitzek, et al., *Proc. CIRP* **2019**, *80*, 126–131.
[181] J.-H. Schünemann, et al., *ECS Trans.* **2016**, *73*(1), 153.
[182] F. Arshad, et al., *Resour. Conserv. Recycl.* **2022**, *180*, 106164.
[183] A. M. Domingues, R. G. de Souza, *Next Sustainability* **2024**, *3*, 100032.
[184] X. Lai, et al., *eTransportation* **2022**, *12*, 100169.
[185] S. Ahmed, et al., *Parametric Study of Lithium-Ion Batteries using BatPaC*, Argonne National Laboratory (ANL)Argonne, IL (United States) **2023**.
[186] P. A. Nelson, et al., Modeling the Performance and Cost of Lithium-Ion Batteries for Electric-Drive Vehicles, Argonne National Lab.(ANL), Argonne, IL (United States), **2019**, No. ANL/CSE-19/2.
[187] M. R. B. Domalanta, et al., *Chem. Eng. Trans.* **2022**, *94*, 139–144.
[188] F. Duffner, et al., *Renew. Sustain. Energy Rev.* **2020**, *127*, 109872.
[189] F. Wang, Y. Deng, C. Yuan, *Procedia Manuf.* **2020**, *49*, 24–31.
[190] J. Sadhukhan, M. Christensen, *Energies* **2021**, *14*(17), 5555.
[191] M. Gutsch, J. Leker, *J. Energy Storage* **2022**, *52*, 105030.
[192] R. Turconi, A. Boldrin, T. Astrup, *Renew. Sustain. Energy Rev.* **2013**, *28*, 555–565.
[193] J. F. Peters, et al., *Renew. Sustain. Energy Rev.* **2017**, *67*, 491–506.
[194] J. Li, et al., *J. Energy Storage* **2023**, *65*, 107306.
[195] S. R. Golroudbary, D. Calisaya-Azpilcueta, A. Kraslawski, *Procedia CIRP* **2019**, *80*, 316–321.
[196] A. Rahman, R. Afroz, *Intern. J. Energy Technol. Pol.* **2017**, *13*(3), 278–291.
[197] F. Degen, et al., *Nat. Energy* **2023**, *8*(11), 1284–1295.
[198] G. Patry, et al., *Energy Sci. Eng.* **2015**, *3*(1), 71–82.
[199] S.-H. Kang, et al., *J. Electrochem. Soc.* **2011**, *158*(8), A936.
[200] M. Wentker, M. Greenwood, J. Leker, *Energies* **2019**, *12*, DOI: 10.3390/en12030504.
[201] J. Schnell, et al., *Energy Technol.* **2020**, *8*(3), 1901237.
[202] R. E. Ciez, J. F. Whitacre, *J. Power Sources* **2017**, *340*, 273–281.
[203] P. A. Nelson, et al., *J. Power Sources* **2015**, *283*, 506–516.
[204] J. F. Peters, A. Peña Cruz, M. Weil, *Batteries* **2019**, *5*(1), 10.
[205] IEA Battery demand by region, 2016–2022, IEA, Paris, France https://www.iea.org/data-and-statistics/charts/battery-demand-by-region-2016–2022, Licence: CC BY 4.0. **April 2023**.

Manuscript received: August 11, 2024
Revised manuscript received: October 8, 2024
Accepted manuscript online: October 9, 2024
Version of record online: November 11, 2024